Chapter 3

Thermal degradation and kinetic study of Bambusa *tulda* and petcoke pyrolysis

3.0 Introduction

The kinetic study provides valuable insights into the decomposition patterns, chemical reaction rates, and various factors influencing the thermal decomposition behavior during pyrolysis. In the context of biomass pyrolysis, kinetic analysis typically involves determining the relevant kinetic parameters and identifying the mechanisms involved in the thermal conversion of biomass. Understanding these mechanisms allows for better regulation of reactions in industrial settings, improved process design, and optimized product yield [41]. Furthermore, this understanding can aid in identifying the properties of biomass that can be effectively utilized for sustainable bioenergy generation or as a substitute for fossil fuels [38]. The kinetic study of biomass focuses on three key factors: activation energy (E_a), pre-exponential factor (A), and kinetic model $f(\alpha)$. Thermogravimetric analysis (TGA) is the most commonly used technique for investigating the kinetics of biomass pyrolysis, providing insights into the solid-phase degradation of lignocellulosic biomass [42, 47]. Many researchers have used CO_2 as a gas agent in addition to N_2 to understand the kinetic mechanism, biochar reactivity, and structural properties. The role of these gas agents in biomass degradation is complex and is influenced by several factors, including feedstock type, reactor design, and process parameters [117]. While some studies suggest that gas agents can facilitate biomass degradation, others indicate that they may not significantly affect the process [118]. Consequently, the claim that the presence of CO_2 will lead to enhanced product quality lacks accuracy without a thorough comparative analysis.

This chapter published in
Bora, A., Choudhury, N.D., Muigai, H. H., Roncancio, R., Gore, J. P. and Mahapatra, S. Experimental and kinetic analysis of Bambusa tulda pyrolysis in carbon dioxide and nitrogen atmosphere. ***Industrial Crops and Products****, 222:119806, 2024.*

Biochar is a carbon-rich material produced through pyrolysis, a thermochemical process that involves converting biomass in an oxygen-limited atmosphere [57]. Due to its versatile properties, biochar has attracted interest in energy research and various industrial sectors. Its applications span a wide range of fields, including generation of syngas through gasification, serving as a substitute for fossil fuels in industrial contexts, or using them as construction materials. Additionally, biochar plays a significant role in environmental applications, such as soil remediation, carbon sequestration, and soil amendment. Biochar is emerging in agriculture for soilless cultivation and industrial applications such as filtering medium or as filter or pigment in plastic production as a substitute of carbon black [119]. Biochar is generally produced by thermally decomposing biomass under inert gases, mostly nitrogen, in a reactor. However, recent studies have indicated that using CO_2 as a purging gas presents several advantages, including increased reactivity and altered physicochemical properties of the resulting biochar. Utilizing CO_2 as a pyrolysis medium is energy-efficient and environmentally sustainable, as it requires no external energy and emits no pollutants due to its complete recirculation within the integrated pyrolysis process [40, 120]. Furthermore, producing biochar in the presence of CO_2 results in a more aromatic and thermally stable material thereby enhanced both the energy yield and energy density of the process [120]. The utilization of biomass and CO_2 provides the benefits of affordable renewable energy to climate change mitigation, aligning synergistically with the goals of Sustainable Development Goal 7 (SDG 7) and Sustainable Development Goal 13 (SDG 13).

The primary objective of this study is to enhance our understanding of the pyrolysis environment affecting the thermochemical conversion of B. *tulda* and determine the kinetic triplets, which include activation energy, pre-exponential factor, and kinetic model. Thermogravimetric analysis (TGA) of B. *tulda* is conducted under N_2 and CO_2 atmospheres and used three model-free methods: Friedman, Flynn-Wall-Ozawa, and Kissinger-Akahira-Sunose for the kinetic study. Another aim of this research is to investigate the physicochemical properties and characterize the biochar produced from the pyrolysis of B.

tulda in a fixed-bed pyrolysis system under N_2 and CO_2 atmospheres. B. *tulda*, a woody bamboo biomass native to Northeast India, is a promising source of energy production due to its rapid growth and high productivity [50, 121]. Understanding the behavior of B. *tulda* during the pyrolysis process is essential as pyrolysis serves as the foundational phase for all thermochemical conversion processes and the output products can be further upgraded depending on their intended applications. Various analytical techniques are used to evaluate the physicochemical, structural, and elemental properties of B. *tulda* char. Overall, the collected data will assist researchers to identify the key characteristics of B. *tulda* and contribute to the development of biofuel based technologies, offering a sustainable alternative to traditional fossil fuels.

3.1 Results and discussion

3.1.1 Effect of CO_2 and N_2 on thermal degradations of *B. tulda*

The thermo-gravimetric analyser is used to measure the mass loss (TG) and mass loss rate (DTG) of B. *tulda* at four different heating rates (10, 20, 30, and 40 K min^{-1}) in N_2 and CO_2 atmosphere within a temperature range of 303 K to 1273 K, as shown in Fig. 3.1. As the temperature increases, the TG profile shows a decrease, indicating an increase in the mass degradation of B. *tulda*. This thermal degradation is characterized by three distinct stages:

- Stage 1 Moisture vaporization: In this stage, weight loss occurs due to the removal of moisture and light volatile compounds within the temperature range of 273−430 K.
- Stage 2 Major devolatilization: In this stage, rapid weight loss occurs due to the removal of low molecular weight lignocellulosic compounds within the temperature range of 430−670 K
- Stage 3 Char formation/continuous minor devolatilization: In this stage, char formation occurs along with the continued release of secondary gases at temperatures up to 1273 K.

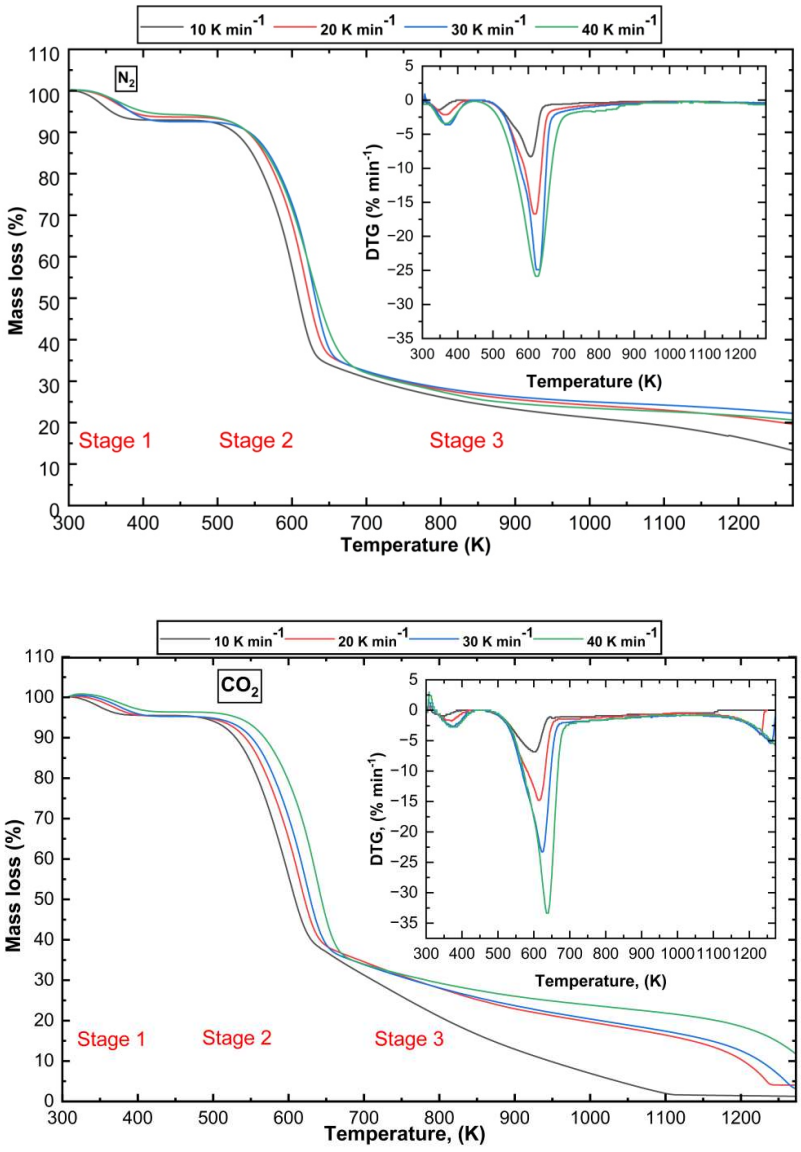

Fig. 3.1 TG and DTG profiles of bamboo at various heating rates using N_2 and CO_2 atmosphere

Stage 1 of the thermal degradation, extended to a temperature of 430 K, and is attributed to moisture evaporation and the breakdown of light organic components. This stage accounts for approximately 10% of the weight loss in B. *tulda*. The primary process of pyrolysis, known as devolatilization, occurs in Stage 2 at temperatures ranging from 455 K to 710 K across all heating rates, both under both N_2 and CO_2 environments. A significant amount of weight loss is observed during this stage due to the thermal degradation of low molecular weight lignocellulosic compounds, including hemicellulose, cellulose, and a small fraction of lignin

[122]. Continuous exposure to heat causes higher molecular weight compounds, such as oligomeric components derived from the depolymerization of hemicellulose, cellulose, and lignin, to further break down into lower molecular weight compounds. These products include phenols, acids, aldehydes, and ketones [123]. Hemicellulose degrades within the temperature range of 430 K to 553 K. In contrast, cellulose degrades at a higher temperature range of 553 K to 670 K. Lignin begins to degrade at lower temperatures and continues to persist up to approximately 1273 K, albeit at a slower rate. The high thermal stability of lignin makes its degradation process more complex compared to that of hemicellulose and cellulose. In Stage 3, continuous devolatilization of char occurs, resulting in a marginal weight loss of up to 1270 K [42]. The distinct occurrence of these three stages is observed under both N_2 and CO_2 atmospheres. However, in the DTG curve under CO_2 atmosphere, a secondary peak appears in Stage 3 between 1250 K and 1270 K. High temperatures above 993 K facilitate the Boudouard reaction, ($C + CO_2 = 2CO$), leading to mass loss during this stage. This reaction acts as an oxygen donor to the generated biochar, promoting the formation of CO during the pyrolysis process [124, 125]. The CO_2 atmospheric conditions lead to more significant weight loss than nitrogen (N_2) atmosphere. At one pressure atmosphere, the average weight loss is approximately 80 % across temperatures ranging from 303 K to 1273 K, under nitrogen environment. However, under CO_2 environment, the weight loss is around 95%. This difference can be attributed to specific gas-phase reactions and carbon fuel consumption caused by the presence of reactive species (CO_2). Additionally, these reactive species may interact with and break down certain tar compounds, which inhibits polymerization and the formation of secondary char. As a result, there is a higher mass loss during the thermal decomposition of *B. tulda* than in an inert nitrogen environment [120,126].

The thermal degradation characteristics of the B. *tulda* and petcoke blend are analysed using Thermogravimetric Analysis (TGA) and Differential Thermogravimetric (DTG) profiles at

heating rates of 10, 20, 30, and 40 K min^{-1}, as shown in Fig. 3.2. Similar to the findings for the B100P0 blend, the B80P20, B60P40, and B40P60 blends also exhibited a three-phase thermal degradation pattern. The initial weight loss, observed below 473 K, is primarily attributed to moisture evaporation. In the temperature range of 573 to 723 K, under CO_2 atmosphere, a noticeable weight change of approximately 1 % occurs, likely due to the thermal expansion of the sample. In contrast, the B0P100 blend (100 % petcoke) demonstrated a two-phase thermal degradation, which can be attributed to its low volatile content (9.87 %), resulting in the absence of a distinct pyrolysis phase. The low reactivity of petroleum coke is attributed to its predominantly aromatic structure and a high aromatic-to-aliphatic ratio. Aromatic carbon atoms are generally less reactive than aliphatic carbons, contributing to the observed thermal behaviour [77]. Low reactivity of petroleum coke is also attributed to the low porosity, compared to biomass char. Porous structure helps reactant (CO_2 here) to diffuse inside and create higher reaction sites.

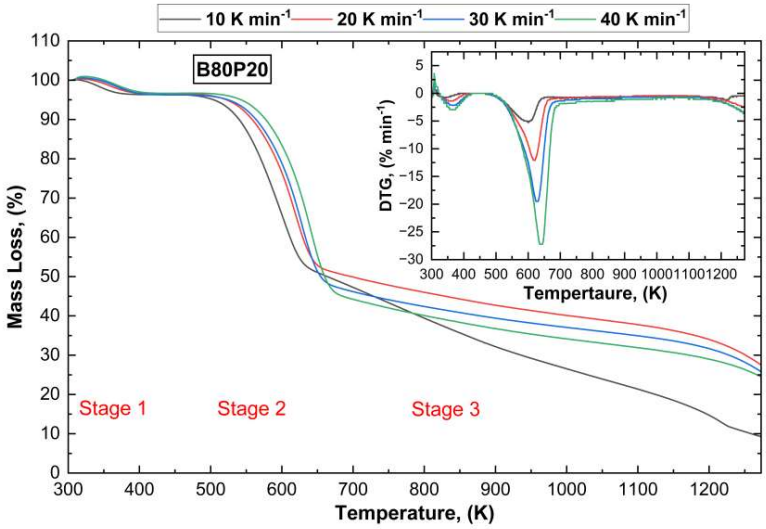

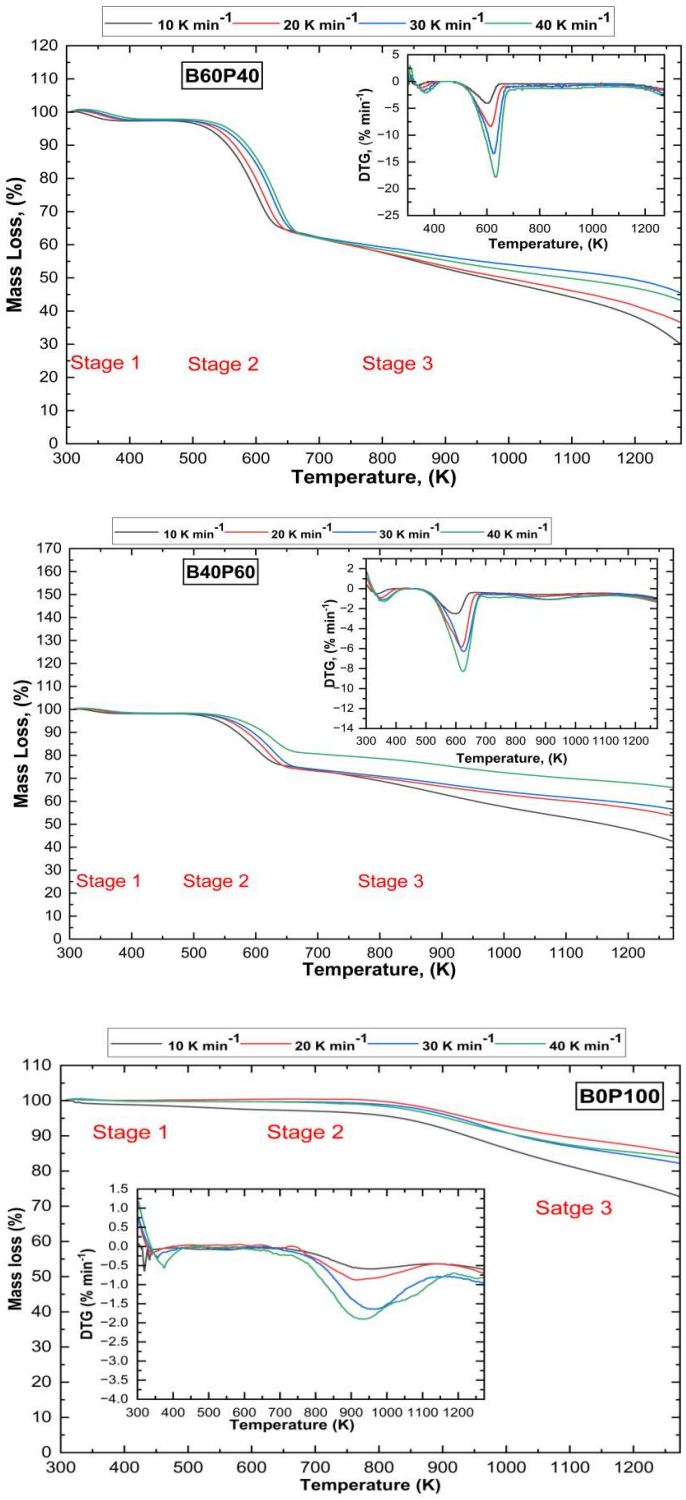

Fig. 3.2 TG and DTG profile for B80P20, B60P40, B40P60, and B0P100 under CO_2 atmosphere

The thermal degradation behavior of B. *tulda* and petcoke occurs in distinct temperature zones, which reflect their difference in compositions and decomposition characteristics. The thermogravimetric (TG) profile indicates that significant mass loss in B. *tulda* blends predominantly occurs during the second stage of degradation, specifically within the lower temperature range of 350 K to 650 K. Within this range, the mass loss is substantial: approximately 50 % for the B80P20 blend, 65 % for the B60P40 blend, and 74 % for the B40P60 blend. This trend indicates an increase in mass loss as the proportion of petcoke decreases, highlighting the influence of biomass content on the thermal decomposition process. Petcoke is characterized by its high fixed carbon content, low oxygen and hydrogen levels, and relatively uniform composition. It undergoes a slower and more gradual thermal degradation process. The carbonization of petcoke begins at higher temperatures, typically between 650 K and 1200 K, and follows a single-step degradation pattern [127]. In contrast, for the species B. *tulda*, nearly 60 % of the total mass loss occurs below 650 K, indicating a rapid devolatilization and thermal degradation within this lower temperature range. Conversely, petcoke experiences only about 5 % of its mass loss below 650 K, demonstrating its resistance to thermal degradation at the lower temperatures. The significant mass loss observed in petcoke, occurs at higher temperatures above 650 K, which aligns with its delayed and slower thermal degradation behavior. This distinct thermal degradation pattern is attributed to the higher fixed carbon content in petcoke, which requires elevated temperatures for breakdown. The differences in thermal behavior between B. *tulda* and petcoke underscore the importance of understanding the specific thermal properties of each component when analysing their blends. These insights are crucial for optimizing thermal conversion processes, especially in applications that involve mixed biomass and petcoke fuel sources.

3.1.2 Effect of heating rates

The heating rate is a crucial factor in the devolatilization of fuel particles. Analysing the thermal decomposition process offers insights into thermochemical conversion mechanisms

at various heating rates [48]. This section examines the effect of four different heating rates on the devolatilization characteristics of B. *tulda* fuel samples. The key parameters for equation 2.4 are derived from the DTG profiles and summarized in Table 3.1. Analysing the DTG plot (Fig. 3.1) reveals that higher heating rates result in characteristic temperatures (e.g., T_i, T_p, $\Delta T_{1/2}$and T_f) shifting to higher temperature regions while not changing the overall thermal degradation trend. This shift occurs because the reduced residence time at ambient temperatures, combined with increasing heating rates, decreases the thermal gradient between the surface and the inner core of the sample particles. This phenomenon leads to thermal hysteresis. The pyrolysis process and the associated degradation reaction kinetics are complex and potentially generating resistance at low heating rates. A lower heating rate allows volatile materials to remain in the reactor for a longer residence time. This extended residence time enables thermal gradients to penetrate the inner core of the particles, facilitating secondary reactions such as cracking, re-polymerization, and re-condensation, which ultimately increases char formation [46, 128]. During the devolatilization of B. *tulda* samples in a nitrogen atmosphere, the rates of mass loss and the characteristic temperatures are nearly identical to those observed in CO_2 environments under the same conditions. This similarity suggests that both gases act as carrier gases during devolatilization.

Table 3.1 Pyrolysis characteristics of B. *tulda* at different heating rates

	Active pyrolysis zone								
Atmosphere	β (K min^{-1})	T_i (K)	T_p (K)	T_f (K)	Mass loss (%)	$-R_p$ (% min^{-1})	$-R_v$ (% min^{-1})	$\Delta T_{½}$ (K)	D_i (% K^{-3} min^{-2})
N_2	10	464.93	606.78	653.7	63.68	8.31	2.84	98.90	8.46×10^{-7}
	20	474.22	618.13	673.93	63.66	16.68	5.96	105.67	3.20×10^{-6}
	30	482.57	628.26	685.38	64.05	26.25	8.17	115.60	6.11×10^{-6}
	40	484.57	625.88	710.18	66.59	27.86	11.1	127.33	8.01×10^{-6}
CO_2	10	455.70	601.18	652.78	61.60	6.87	2.93	89.21	8.24×10^{-7}
	20	470.12	614.92	665.33	61.12	14.83	5.67	90.58	3.21×10^{-6}
	30	478.45	622.74	678.45	62.86	22.93	8.41	93.85	6.89×10^{-6}
	40	490.93	638.13	692.67	65.57	33.36	12.26	105.87	1.23×10^{-5}

The devolatilization index measures the efficiency of a thermal conversion process [50]. A higher devolatilization index indicates a greater conversion of B. *tulda* into biochar, while lower values suggest a higher loss of B. *tulda* as gaseous byproducts. Increasing the heating rate during the thermal conversion process can improve the devolatilization index by accelerating the overall process and reducing the duration of high-temperature exposure, thereby minimizing product loss. Furthermore, the devolatilization index can serve as a parameter to identify opportunities for enhancing overall process performance. The study evaluated the devolatilization indices (D_i) of blends of B. *tulda* and petcoke at various ratios and four heating rates presented in Table 3.2, providing a comprehensive understanding of the thermal conversion process of these fuel samples.

Table 3.2 Pyrolysis characteristics of B. *tulda* and petcoke at different heating rates

	Active pyrolysis zone								
Fuel samples	β (K min^{-1})	T_i (K)	T_p (K)	T_f (K)	Mass loss (%)	$-R_p$ (% min^{-1})	$-R_v$ (% min^{-1})	$\Delta T_{½}$ (K)	D_i (% K^{-3} min^{-2})
B80P20	10	486.86	599.15	649.50	44.74	5.04	2.75	56.7	8.38×10^{-7}
	20	495.20	615.7	667.38	44.79	12.06	5.2	81.30	2.53×10^{-6}
	30	498.6	628.65	680.57	48.85	19.50	8.05	88.32	5.67×10^{-6}
	40	501.07	636.13	693.22	52.20	27.24	10.83	97.78	9.47×10^{-6}
B60P40	10	494.07	601.15	648.83	32.36	4.02	2.08	58.44	4.82×10^{-7}
	20	499.14	615.77	660.90	33.64	8.34	4.16	62.51	1.81×10^{-6}
	30	498.53	622.10	679.42	34.30	13.38	5.67	84.05	2.91×10^{-6}
	40	499.42	636.97	688.15	35.32	17.82	7.48	84.55	4.96×10^{-7}
B40P60	10	495	600.70	654.73	22.65	2.50	1.42	48.15	2.48×10^{-7}
	20	483.37	617.42	671.37	24.39	5.86	2.59	79.63	6.39×10^{-7}
	30	484.45	622.05	688.14	23.82	6.30	3.52	95.63	7.70×10^{-7}
	40	488.85	623.75	689.40	25.57	8.27	2.63	84.95	8.39×10^{-7}

It specifically focuses on the devolatilization behavior at three different B. *tulda* to petcoke ratios: B80P20, B60P40, and B40P60.As the percentage of petcoke increases, there is a significant rise in the devolatilization index, indicating improved thermal conversion. For the B80P20 blend, the devolatilization indices at heating rates of 10, 20, 30, and 40 K min^{-1} are

8.38×10^{-7}, 2.53×10^{-6}, 5.67×10^{-6}, and 9.47×10^{-7}, respectively. These values illustrate a greater release of volatiles as the heating rate increases, emphasizing thermal conversion efficiency at higher rates. In contrast, the B60P40 samples exhibit devolatilization indices of 4.82×10^{-7}, 1.81×10^{-6}, 2.91×10^{-6}, and 4.96×10^{-7} across the same heating rates. This range indicates a moderate increase in volatile release, with a noticeable decrease occurring at the higher heating rate. This variation may be attributed to different thermal decomposition dynamics present in this blend. For the B40P60 fuel samples, the indices are 2.48×10^{-7}, 6.39×10^{-7}, 7.70×10^{-7}, and 8.39×10^{-7}, respectively. These lower values suggest a reduced release of volatiles, which correlates with the increased petcoke content. This indicates a slower devolatilization process due to the higher fixed carbon content in petcoke. These findings highlight the crucial role of blending fuel samples and the impact of heating rates on the devolatilization process. Blends with higher petcoke content and increased heating rates lead to accelerated devolatilization, potentially resulting in a greater yield of biochar. Consequently, the devolatilization index is an important parameter for optimizing thermal conversion processes. Understanding the relationship between blend ratios, heating rates, and devolatilization efficiency makes it possible to minimize product loss, enhance the performance of the conversion process, and improve the overall efficiency of thermal conversion systems.

3.1.3 Kinetic analysis

Thermogravimetric Analysis (TGA) experiments play a crucial role in understanding the thermochemical conversion of biomass by analysing mass loss and mass loss rates. This analysis provides valuable insights into the conversion process. The key parameters in this study include the kinetic triplet: activation energy, pre-exponential factor, and kinetic model. A comprehensive understanding of these parameters is vital, as it can contribute in optimization subsequent thermochemical conversions of biomass after pyrolysis and enhance the utilization of biomass resources for sustainable energy production.

3.1.3.1 Determination of activation energy

Activation energy is a fundamental concept in chemical kinetics. It represents the minimum amount of energy required for a chemical reaction to initiate. Reactions with lower activation energies tend to proceed more quickly, whereas those with higher activation energies precede slower [129]. In this study, the activation energies for B. *tulda* are determined using linear regression based on iso-conversional plots (Equations 2.11-2.13) for different conversion levels (α), which varied from 0.1 to 0.8 in increments of 0.1. The activation energies obtained from three iso-conversional methods (Friedman, FWO, and KAS) is presented in Fig. 3.3 - 3.5. All methods demonstrated suitability for the experimental data, with correlation coefficients (R^2) exceeding 0.9. This signifies the reliability and validity of the iso-conversional methods used in this study for estimation of the activation energy [130].

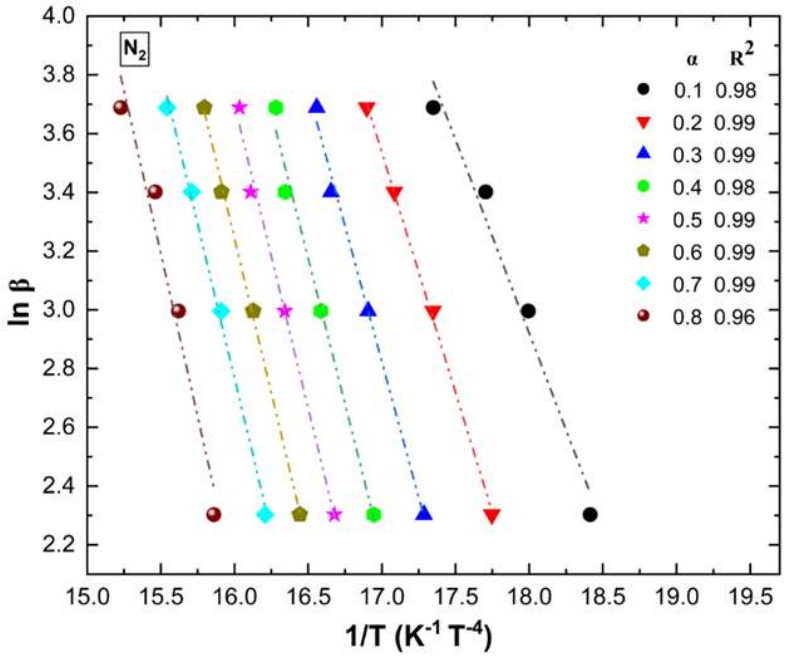

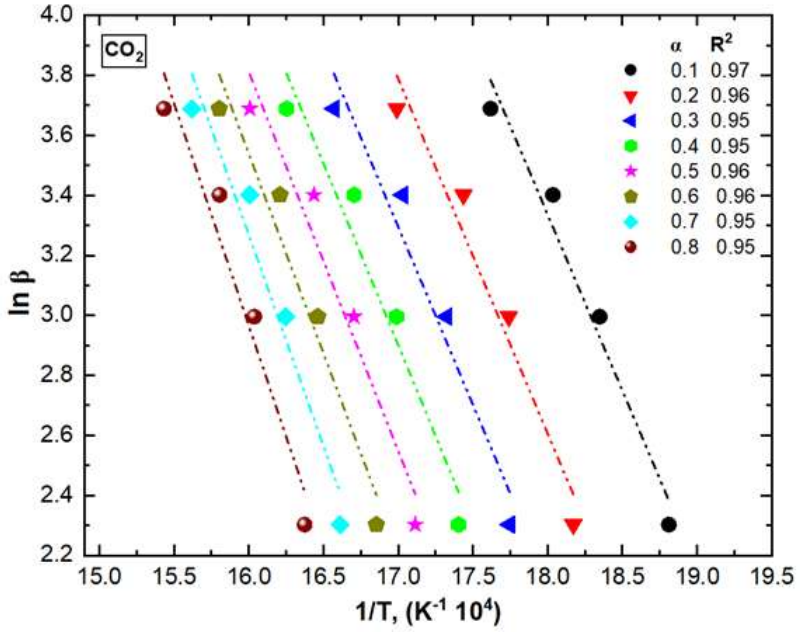

Fig. 3.3 Linear relationship between $ln\beta$ versus 1/T using FWO model under $N_2$and CO_2 atmosphere

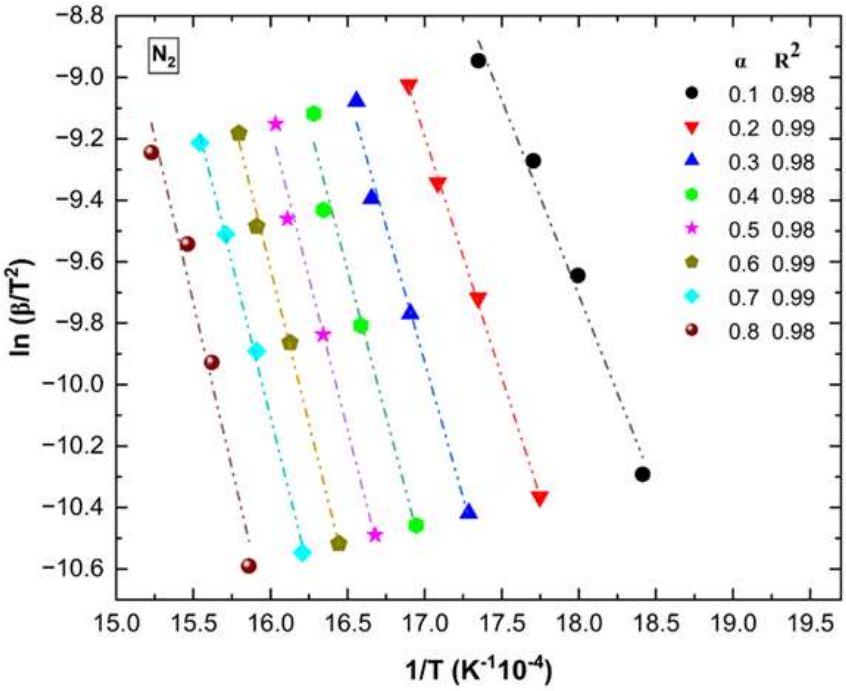

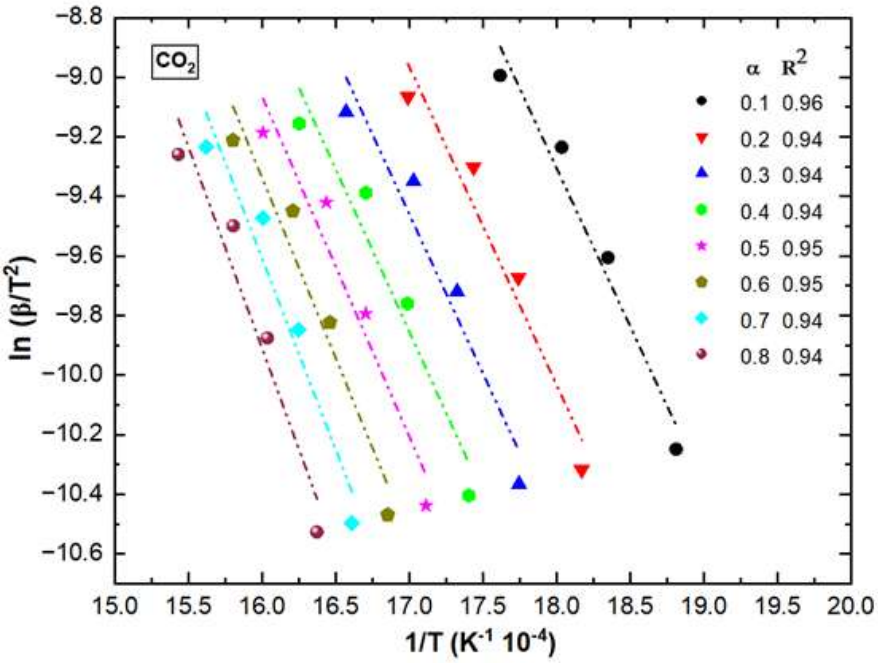

Fig. 3.4 Linear relationship between $ln(\beta/T^2)$ versus 1/T using KAS model under N_2 and CO_2 atmosphere

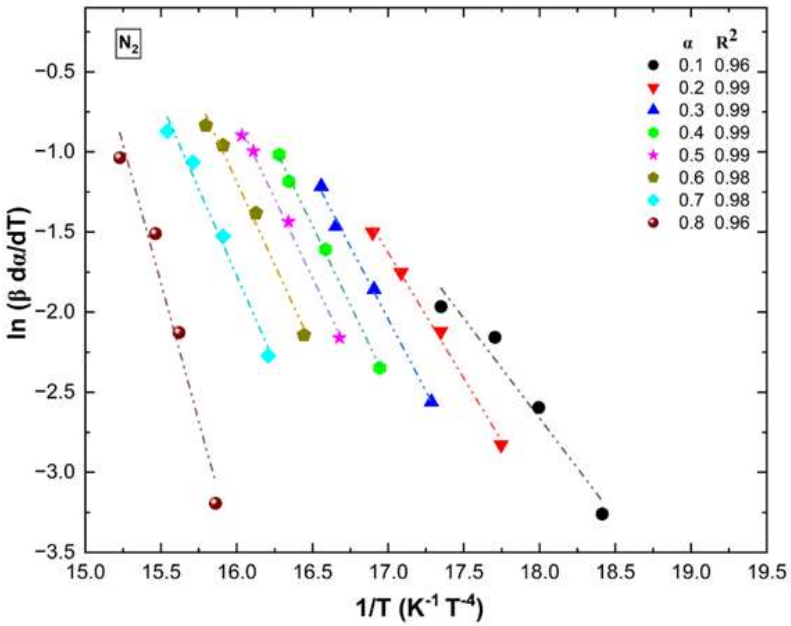

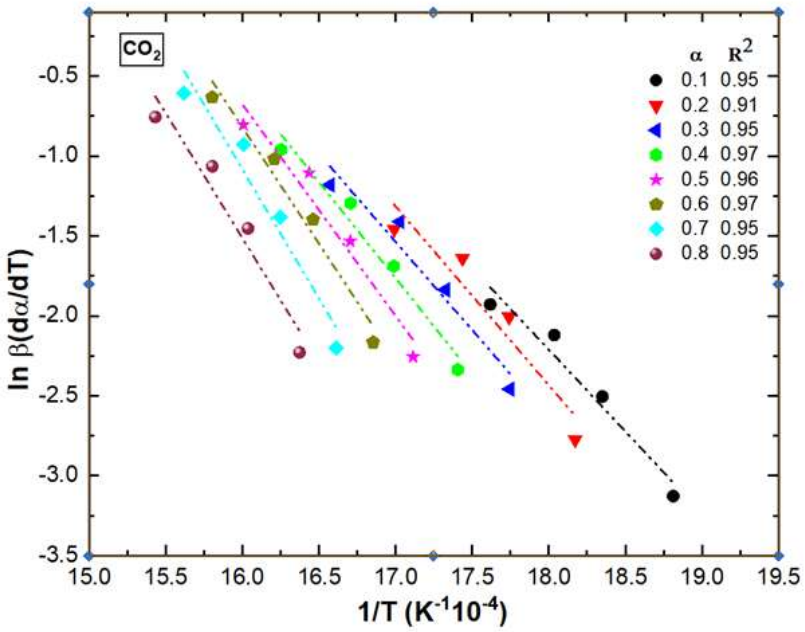

Fig. 3.5 Linear relationship between ln[β(dα/dT)] versus 1/T using Friedman model under N_2 and CO_2 atmosphere

Fig. 3.6 presents the activation energy obtained from each method as a function of conversion. The activation energy varies with conversion (α) as the reaction progresses due to multiple simultaneous reactions that occur during the pyrolysis process, including the dehydration and depolymerization of biomass. This variation in energy requirements contributes to the observed changes in activation energy with the progression of the pyrolysis process [131]. In all iso-conversional methods, the estimated activation energy exhibited a consistent upward trend as conversion (α) increases, rising significantly towards the end of the process in both inert (N_2) and oxidative (CO_2) atmospheres. While the Friedman model indicates non-monotonic variations in the activation energy curve, the FWO and KAS methods display a stable upward trend without fluctuations throughout the conversion process in both atmospheres. This upward trend is consistent with findings reported by other researchers [45, 132].

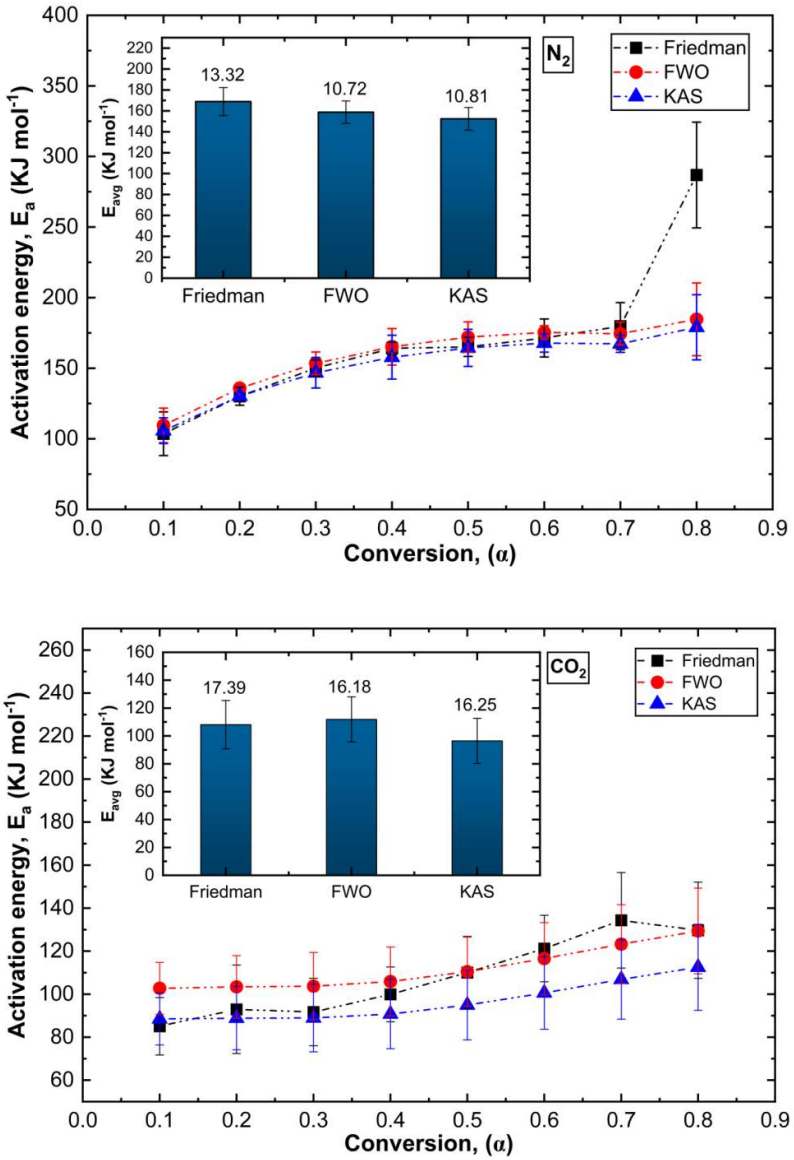

Fig. 3.6 Correlation between activation energy and different conversions under N_2 and CO_2 atmosphere

Table 3.3 provides the estimated activation energies under N_2 and CO_2 atmospheres for the reactions. The increased activation energy with conversion indicates an exothermic breakdown of biomass, often influenced by competing macromolecules and intermolecular interactions. On the other hand, a decrease in activation energy with conversion suggests a subsequent endothermic reaction followed by an irreversible step [133]. This variation in activation energy with conversion provides valuable insights into the kinetic model and the pre-exponential factor, which are essential for understanding and predicting the reaction

rate. Therefore, further investigations are conducted using master plots to compare the experimental kinetic models with theoretical kinetic models of solid-state reactions.

Table 3.3 Activation energy and pre-exponential factor estimated by different iso-conversional methods under N_2 and CO_2 atmosphere

Atmosphere	Conversion α	Friedman		FWO		KAS	
		E_a (kJ mol^{-1})	lnA (min^{-1})	E_a (kJ mol^{-1})	lnA (min^{-1})	E_a (kJ mol^{-1})	lnA (min^{-1})
N_2	0.1	103.59	22.82	109.51	23.89	105.78	23.22
	0.2	130.18	27.63	135.87	28.66	130.29	27.65
	0.3	150.10	31.24	153.48	31.85	146.79	30.64
	0.4	164.08	33.77	165.17	33.96	157.83	32.64
	0.5	165.15	33.96	172.02	35.21	164.46	33.84
	0.6	171.46	35.10	175.37	35.81	167.86	34.45
	0.7	179.80	36.61	174.48	35.65	167.31	34.35
	0.8	286.88	56.01	184.66	37.49	179.01	36.47
CO_2	0.1	85.07	17.99	102.72	21.62	88.51	18.70
	0.2	92.96	19.61	103.39	21.75	88.82	18.77
	0.3	91.69	19.35	103.73	21.82	88.91	18.79
	0.4	99.92	21.04	105.87	22.26	90.75	19.16
	0.5	110.06	23.12	110.44	23.20	94.93	20.02
	0.6	121.23	25.41	116.53	24.45	100.58	21.18
	0.7	134.37	28.11	123.25	25.83	106.84	22.47
	0.8	129.73	27.16	129.38	27.09	112.52	23.63

The activation energy of B. *tulda* is measured under two different atmospheric conditions. The average activation energy values obtained are 160.05 kJ-mol^{-1} and 105.51 kJ-mol^{-1} respectively. These values are within the typical range for lignocellulosic biomass, which is often used in the production of biofuels and other bioproducts. The lower activation energy observed in the presence of CO_2 atmospheric condition suggests that this environment enhances the thermal degradation of biomass, potentially leading to improved yields and better quality products. Further research is needed to confirm and understand the mechanisms underlying this effect. The present study also determined the activation energy of bamboo, which is within the range of values reported in Table 3.4. However, differences in activation energy can arise due to experimental conditions, including the physicochemical

properties of samples, the gas agents used, and the kinetic models applied. Notably, the average activation energy for B. *tulda* is lower than most bamboo samples reported in the literature indicating that it requires less energy for thermal degradation.

Table 3.4 Comparison of activation energy of different bamboo samples

Samples	Gas agent	Methods	Activation energy (kJ mol^{-1})	Reference
Bamboo	N_2	FWO	262.53	[134]
		KAS	266.62	
Indian Bamboo	N_2	Friedman	180.89	[50]
		FWO	154.59	
		KAS	152.52	
B.*tulda*	N_2	Friedman	168.91	Present Study
		FWO	158.82	
		KAS	152.42	
	CO_2	Friedman	108.13	
		FWO	111.91	
		KAS	96.48	

This study investigated the effect of blending petcoke with B. *tulda* on activation energy. The activation energies for the blends B80P20, B60P40, and B40P60 are evaluated at different conversion levels using the Friedman, Flynn-Wall-Ozawa (FWO), and Kissinger-Akahira-Sunose (KAS) iso-conversional methods under CO_2 atmosphere. All the correlation coefficients are higher than 0.95, indicating a high level of consistency in the calculated kinetic parameters, as shown in Fig. 3.7-3.9. The results consistently showed a similar upward trend across all three methods. However, for the blend B0P100, the correlation coefficient was below 0.85; thus, it is excluded from the study.

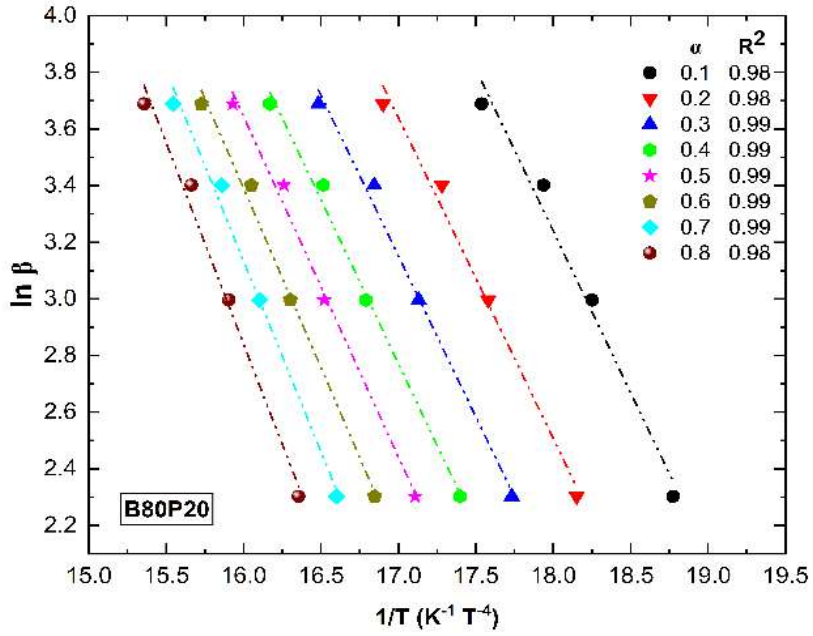
α R²
0.1 0.98
0.2 0.98
0.3 0.99
0.4 0.99
0.5 0.99
0.6 0.99
0.7 0.99
0.8 0.98
B80P20
ln β
1/T (K⁻¹ T⁻⁴)

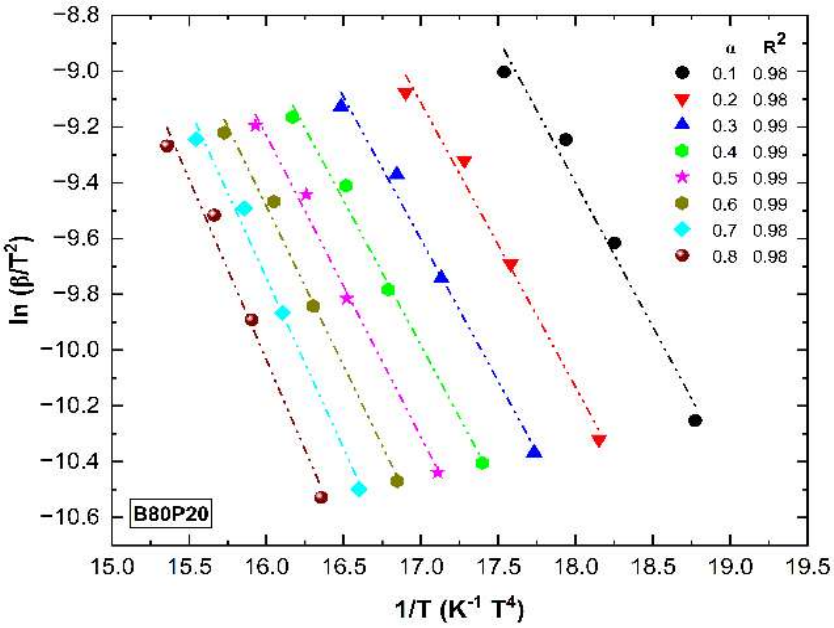
α R²
0.1 0.98
0.2 0.98
0.3 0.99
0.4 0.99
0.5 0.99
0.6 0.99
0.7 0.98
0.8 0.98
B80P20
ln (β/T²)
1/T (K⁻¹ T⁴)

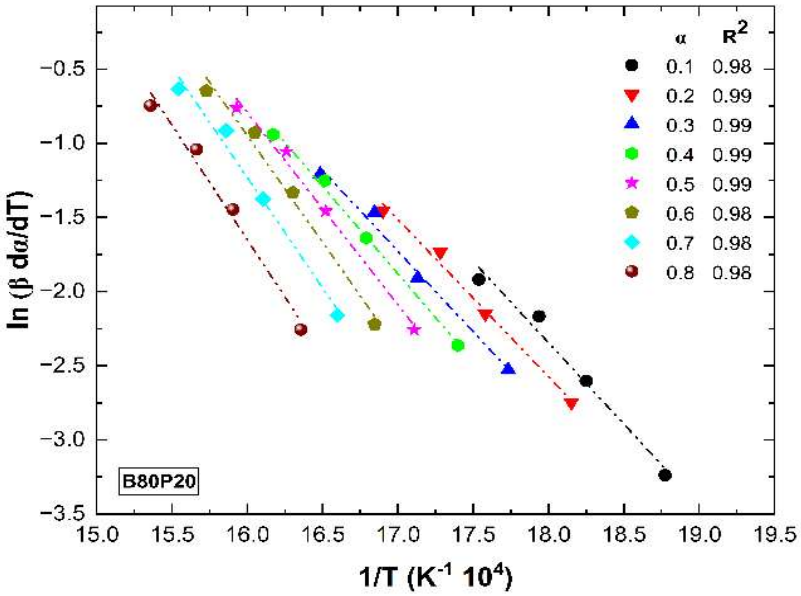

Fig. 3.7 Linear relationship for B80P20 using FWO, KAS model and Friedman methods under CO_2 atmosphere

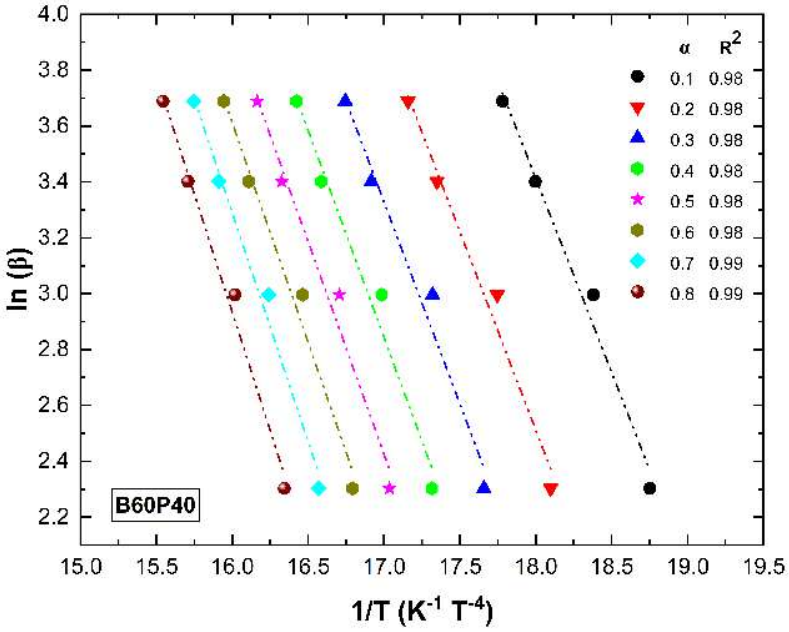

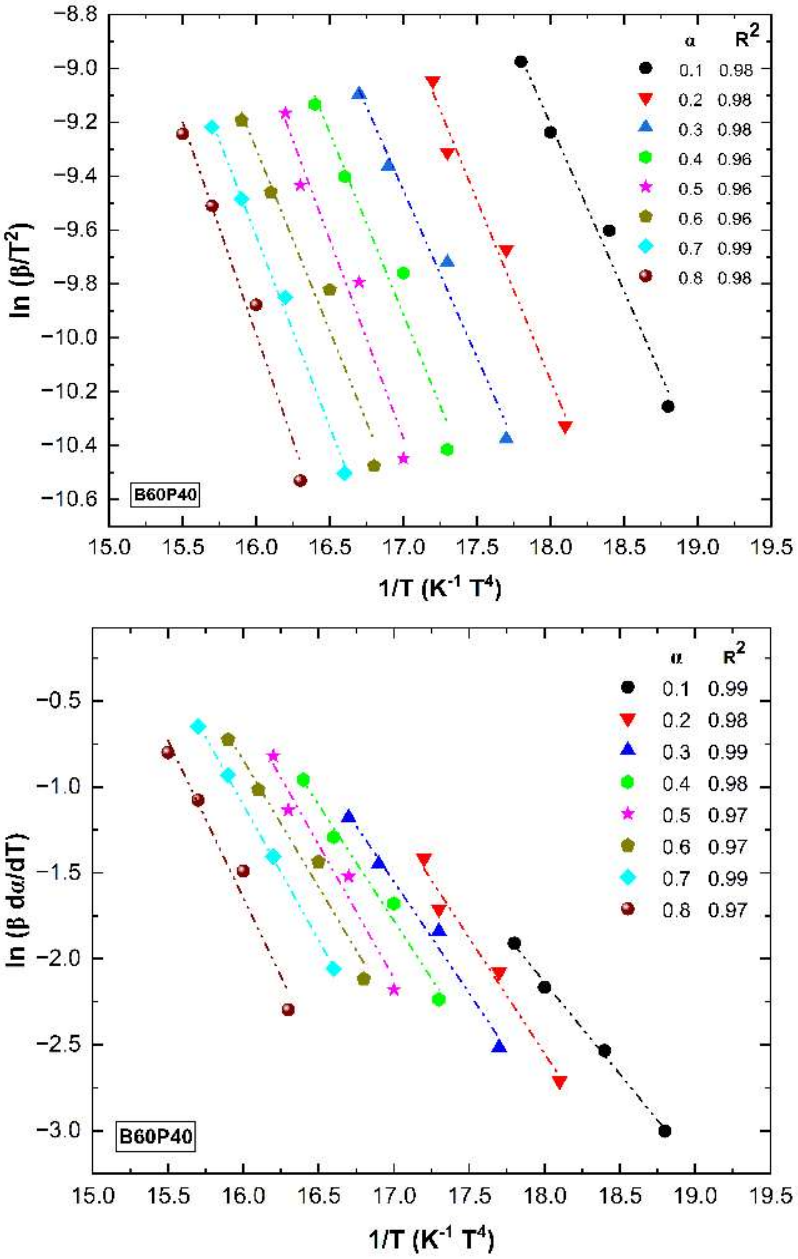

Fig. 3.8 Linear relationship for B60P40 using FWO, KAS model and Friedman methods under CO_2 atmosphere

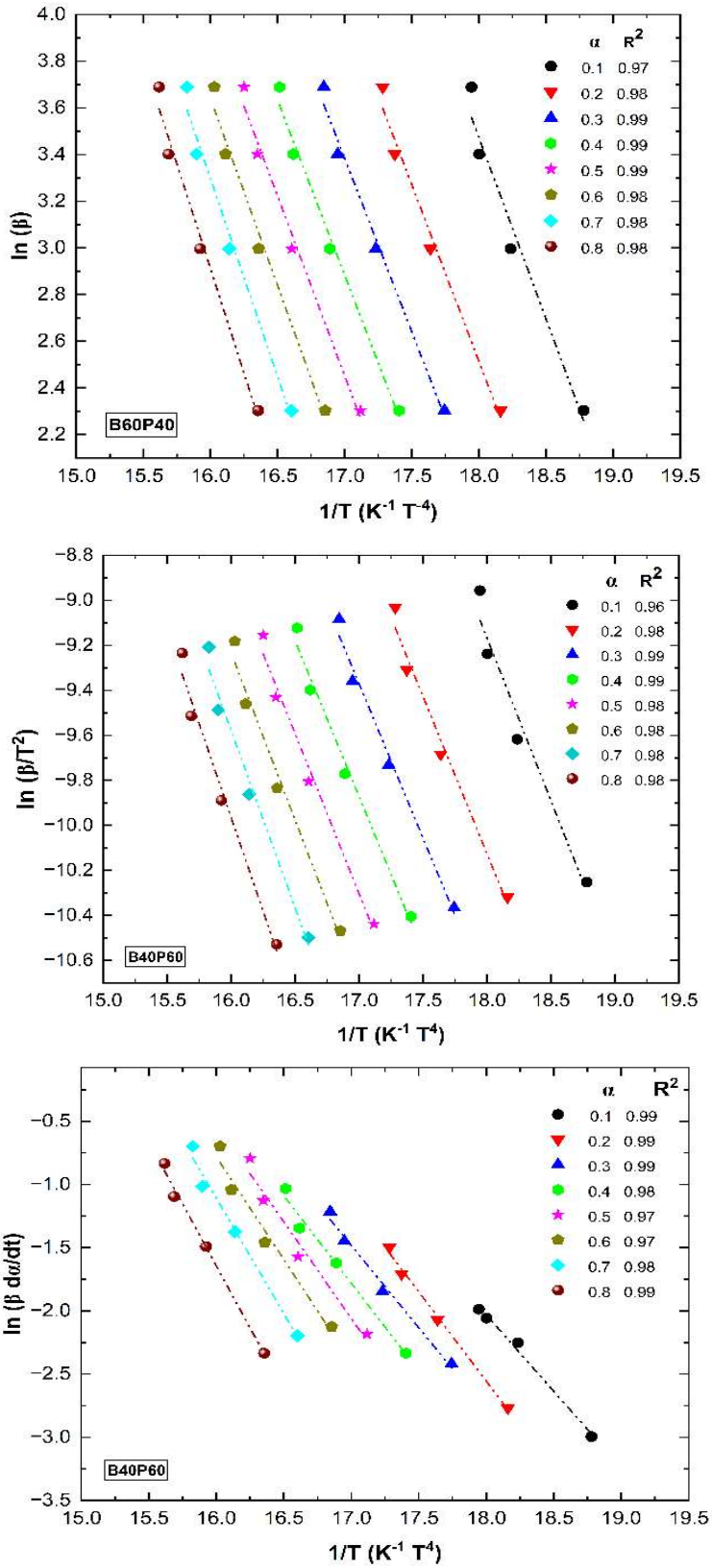

Fig. 3.9 Linear relationship for B40P60 using FWO, KAS model and Friedman methods under CO_2 atmosphere

Fig. 3.10 presents the correlation between activation energy and different conversions of B80P20, B60P40, and B40P60. Four iso-conversional methods (Friedman, FWO, and KAS) are used to determine the activation energy from temperature ranging from room temperature to 1273 K under CO_2 atmosphere. The kinetic plots for the models exhibit a similar pattern, demonstrating that this method is suitable for calculating activation energy. The variations observed with increasing conversion suggest that the thermal decomposition process is not a single-step reaction. Instead, it involves a complex, multi-stage reaction scheme, where different energy levels are required as the reaction progresses. For B80P20, the activation energy increases monotonously with the conversion (α). However, beyond conversion of 0.4 there is a little rise in the profile. This could be due to the prevalent perception that weak chemical bonds cleavage at low temperatures firstly while strong bonds with higher bonding energy are subsequently broken at higher temperatures, i.e., more energy are required at higher conversions. It is also reflected for B60P40 and B40P60 fuel samples with the increase in conversions. However, fluctuations in the E_a vs. α profile observed with the Friedman method for all the fuel samples can be attributed to its dependence on the instantaneous rate of conversion, which is more susceptible to experimental noise. As a result, accuracy of the method is rather reduced, resulting to the variability in the E_a values [135]. The observed increasing and decreasing trends in activation energy with increasing conversion for B60P40 and B40P60 blends reflect the intricate and complex nature of petcoke blended with B. *tulda*. These trends suggest that the reaction mechanism undergoes significant changes, with varying degrees of cracking or volatilization of the blended fuel samples occurring at different temperatures and heating rates. This dynamic behavior confirms the strong dependence of activation energy upon conversion. Since pyrolysis involves different reactions at that occur simultaneously at each point of conversion, each individual reaction contributes to the overall reaction mechanism, highlighting the complexity of the thermal decomposition process [136,137].

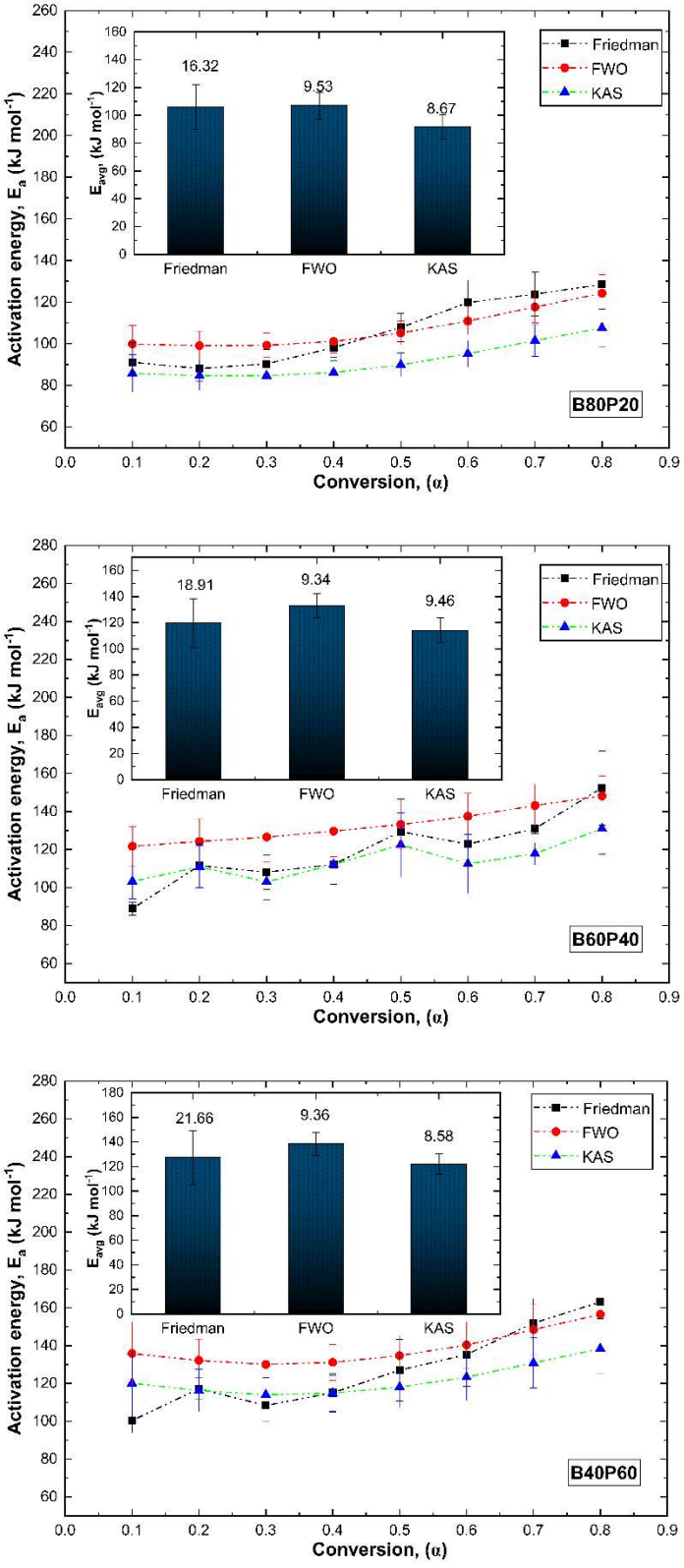

Fig. 3.10 Correlation between activation energy and different conversions under CO_2 atmosphere for B80P20, B60P40, and B40P60 fuel samples

The findings from all three isoconversional methods consistently showed a similar upward trend in activation energy as the petcoke content increased in the blends. Table 3.5 indicates that the activation energy for the B80P20 blend is 101.66 $kJmol^{-1}$, which is lower than that of pure B. *tulda*. As the proportion of petcoke in the blends increases, the activation energy also increases, measuring 122.23 $kJmol^{-1}$ for the B60P40 blend and 129.30 $kJmol^{-1}$ for the B40P60 blend respectively. Despite this increase, the activation energies for these blends remain significantly lower than those for pure B. *tulda* under nitrogen atmosphere. Previous studies indicate that the activation energy for pure petcoke ranges from 200 to 260 $kJmol^{-1}$ [59, 138, 139]. In this study, it is found that blending petcoke with B. *tulda* significantly reduces the activation energy. This decrease can be attributed to the interaction between the two components in the blend. The presence of alkali and alkaline earth metals in B. *tulda* likely enhances the interaction with petcoke, facilitating the thermal degradation process. As a result, this leads to a more efficient conversion of the blended fuel into char. This catalytic effect highlights the potential benefits of blending biomass with petcoke to optimize thermal conversion processes. It highlights the synergistic effects that can be achieved in such blended fuel systems.

Table 3.5 Activation energy and pre-exponential factor estimated by different iso-conversional methods for B80P20, B60P40, and B40P60

Conversion α	Friedman		FWO		KAS	
	Ea (KJ mol^{-1})	lnA (min^{-1})	Ea (KJ mol^{-1})	lnA (min^{-1})	Ea (KJ mol^{-1})	lnA (min^{-1})
B80P20						
0.1	91.141	24.457	99.8654	25.902	85.772	23.568
0.2	88.072	23.949	99.066	25.770	84.687	23.389
0.3	90.339	24.325	99.259	25.802	84.641	23.381
0.4	98.125	25.614	101.061	26.100	86.167	23.634
0.5	107.772	27.212	105.135	26.775	89.882	24.249
0.6	119.761	29.197	110.859	27.723	95.178	25.126
0.7	123.831	29.871	117.626	28.844	101.472	26.168
0.8	128.472	30.640	124.181	29.929	107.560	27.177
B860P40						
0.1	88.909	33.530	121.712	37.3135	103.2171	35.180
0.2	111.562	36.143	124.239	37.604	110.951	36.072
0.3	108.078	35.741	126.568	37.873	103.0314	35.159
0.4	112.201	36.216	129.637	38.227	112.1684	36.212
0.5	129.405	38.200	133.177	38.635	122.4415	37.397
0.6	122.791	37.437	137.487	39.132	112.4114	36.241
0.7	130.976	38.381	143.148	39.785	117.8461	36.867
0.8	152.378	40.849	148.187	40.366	131.0044	38.385
B40P60						
0.1	100.374	31.548	135.799	36.292	120.036	34.181
0.2	117.223	33.804	132.180	35.807	116.269	33.676
0.3	108.374	32.619	130.039	35.520	114.002	33.373
0.4	115.075	33.516	131.162	35.671	114.880	33.490
0.5	127.011	35.115	134.678	36.142	118.061	33.916
0.6	135.27	36.222	140.342	36.900	123.297	34.618
0.7	151.935	38.452	148.422	37.982	130.836	35.627
0.8	163.065	39.943	156.524	39.067	138.390	36.639

3.1.3.2 Determination of kinetic model and pre-exponential factor

Analysing kinetic models is an important step in understanding the mechanisms of chemical reactions. Iso-conversional methods are commonly used in biomass thermal degradation studies to identify the appropriate kinetic model. According to Vyazovkin *et al.* (2011),

assuming a reaction model without thorough verification using master plots may not be reliable [53]. There may be other models that better describe the reaction mechanism. If a reaction model is assumed without proper evaluation, it might misrepresent the reaction, potentially leading to incorrect or misleading conclusions. Therefore, it is essential to carefully assess the kinetic model to ensure it accurately reflects the underlying reaction mechanisms. In this study, the Criado master plot is utilized to predict the kinetic model. Fig. 3.11 shows the normalized conversion $\left(Z(\alpha)\right)$ of B. *tulda* at a heating rate of 10 K min^{-1} under both inert (N_2) and reducing (CO_2) atmospheres. This analysis compares experimental measurements with theoretical solid-state reaction models, which are represented by various expressions of $f(\alpha)$ and $g(\alpha)$ presented in Table 2.2. Since the curves are normalized, the focus is on the similarity of their shapes rather than on the accuracy of the fit. The experimental reduced plot overlaps with one or more master plots across various ranges of conversion (α). For the nitrogen (N_2) atmosphere, the experimental curve aligns with the 3-dimensional diffusion model (D3) from conversions 0 to 0.5. In the range of conversions from 0.6 to 0.7, the curve shows similarities to the nucleation model (A2) and the first-order reaction model (F1). Furthermore, at conversions above 0.7, the curve approaches the second-order reaction model (F2), although it does not completely superimpose on it. On the other hand, the experimental curve for the CO_2 atmosphere aligns with the F2 model for conversions ranging from 0 to 0.1. From 0.1 to 0.5, it closely resembles both the A2 and F1 reaction models. Specifically, at conversions of 0.5 and 0.8, the experimental curve coincides entirely with the D3 model. Above a conversion of 0.8, the curve again shifts closer to the A2 and F1 reaction models.

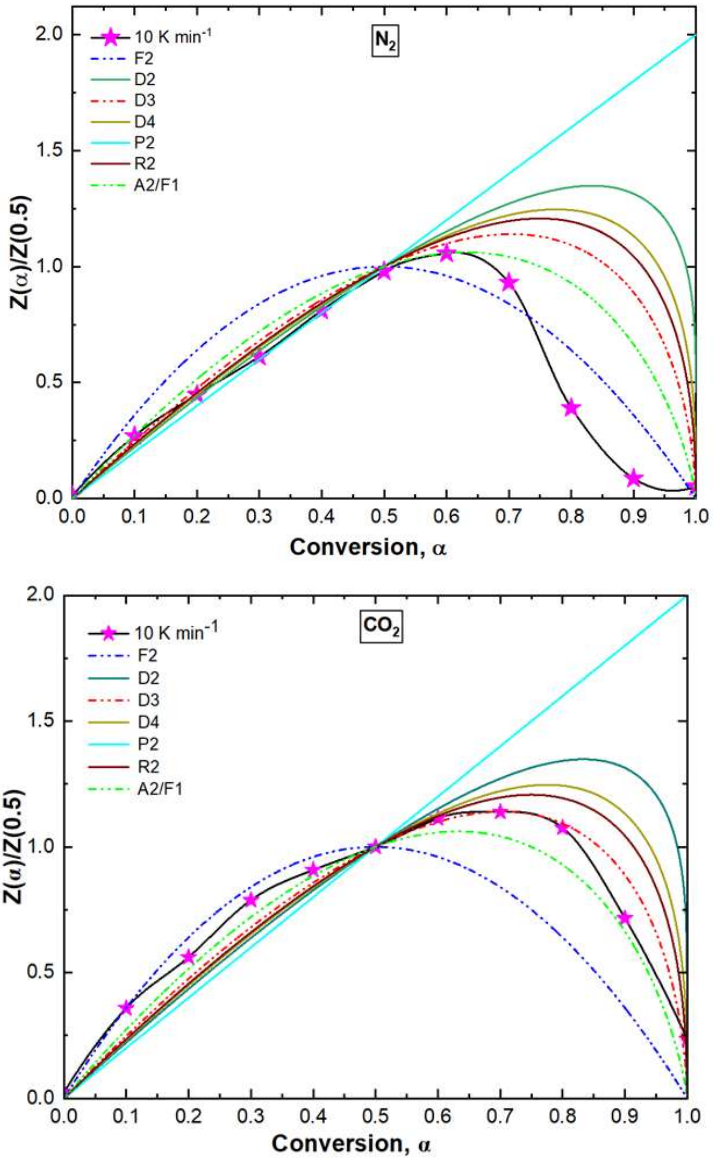

Fig. 3.11 $\frac{Z(\alpha)}{Z(0.5)}$ versus conversion under N_2 and CO_2 atmosphere

The compensation effect is determined using predicted reaction models, which estimate the pre-exponential factor (A) at different conversion rates through iso-conversional methods for nitrogen and carbon dioxide atmospheres, using equations 2.13–2.15. The pre-exponential factor represents the frequency of molecular vibrations involved in a reaction. Table 3.6 presents the compensation parameters for calculating the pre-exponential factors in nitrogen and carbon dioxide atmospheres. The lnA values under N_2 ranged from 22.82 to 56.01 min^{-1}, while for CO_2, it varied from 17.99 to 27.16 min^{-1}. This variation in pre-exponential factors

with conversion indicates that the thermal degradation of B. *tulda* during pyrolysis is complex. Although cellulose and hemicellulose are both polysaccharides, the significant differences in their pre-exponential values highlight the heterogeneity in the structural composition of B. *tulda*. Furthermore, the increase in values of lnA toward α ≥ 0.7 signifies the degradation of remaining lignin and char formation [140].

Table 3.6 Compensation parameter of *B. tulda* for N_2 and CO_2 atmosphere

Compensation Parameters	N_2			CO_2		
	a*	b*	R^2	a*	b*	R^2
F1	0.19093	6.83073	0.9989	0.18987	2.89839	0.9968
F2	0.17248	4.4158	0.9688	0.24051	-2.02898	0.9992
D3	0.20276	-211567	0.9899	0.2444	-5.65309	0.9936
A2	0.15811	7.11669	0.9765	0.14616	6.94023	0.951

Fig. 3.12 illustrates the correlation between activation energy (E_a) and the pre-exponential factor (A) at various conversion fractions (α). The data points demonstrate a strong linear relationship across the range of lower to higher conversion fractions, indicating the presence of the kinetic compensation effect [141]. As temperature increases, the vibrations of the constituent particles intensify, which enhances the bending and stretching of the molecules at the molecular level. This linear relationship between activation energy and the logarithm of the pre-exponential factor aligns with the Arrhenius-type law [142-144]. The high degree of linearity of the fit validates the estimated kinetic parameters effectively.

Fig. 3.13 presents the normalized conversion $Z(\alpha)$ for the compositions B80P20, B60P40, and B40P60, under a heating rate of 10 K-min^{-1} under CO_2 atmospheres. The purpose of this figure is to compare the experimental data with various theoretical solid-state reaction models, which are characterized by different functions of $f(\alpha)$ and $g(\alpha)$, as outlined in Table 2.2. The aim is to determine the reaction mechanism by examining the shape similarities between the experimental curves and the theoretical models rather than relying on precise curve-fitting metrics. The normalized nature of the curves allows us to focus on their shape correspondence across different conversion ranges.

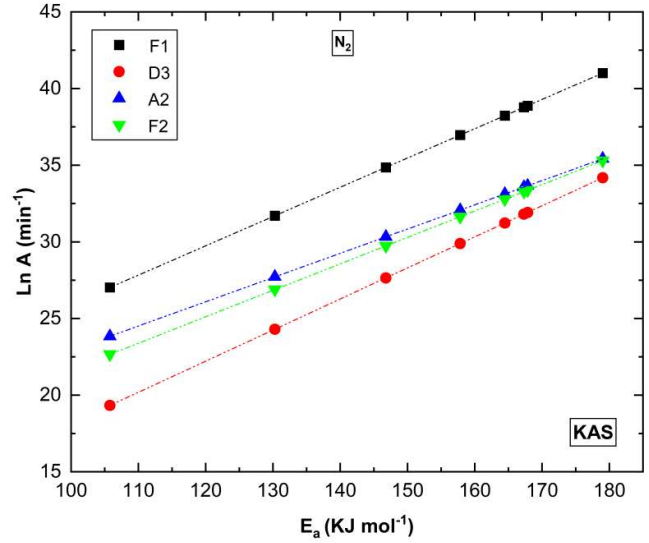
F1
D3
A2
F2
N2
KAS
Ln A (min-1)
Ea (KJ mol-1)

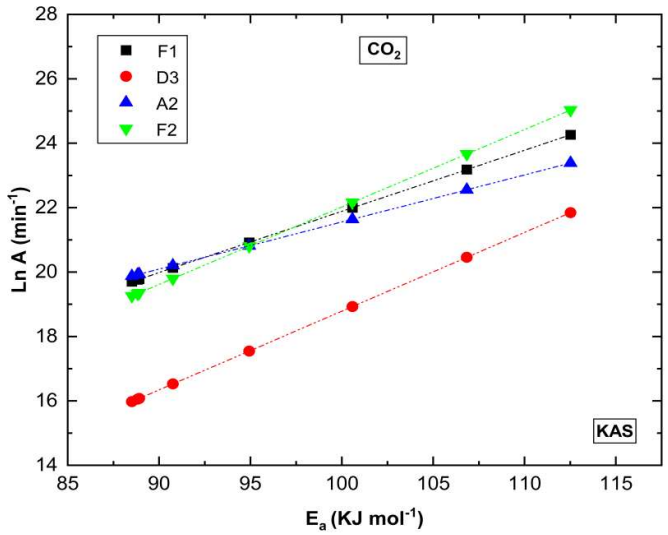
F1
D3
A2
F2
CO2
KAS
Ln A (min-1)
Ea (KJ mol-1)

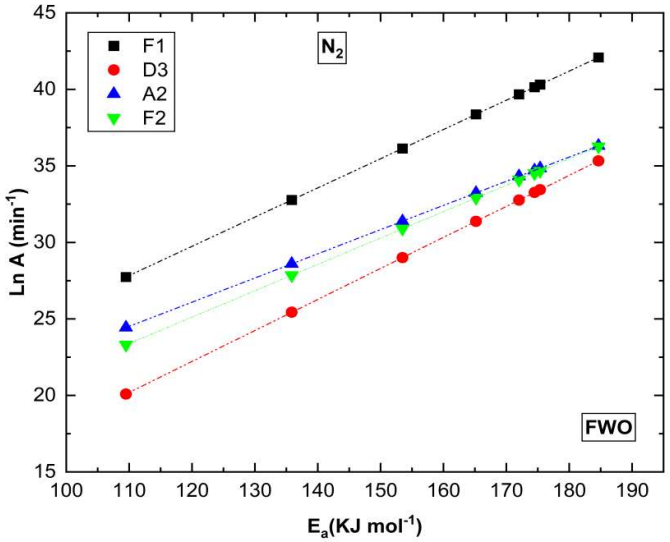
F1
D3
A2
F2
N2
FWO
Ln A (min-1)
Ea(KJ mol-1)

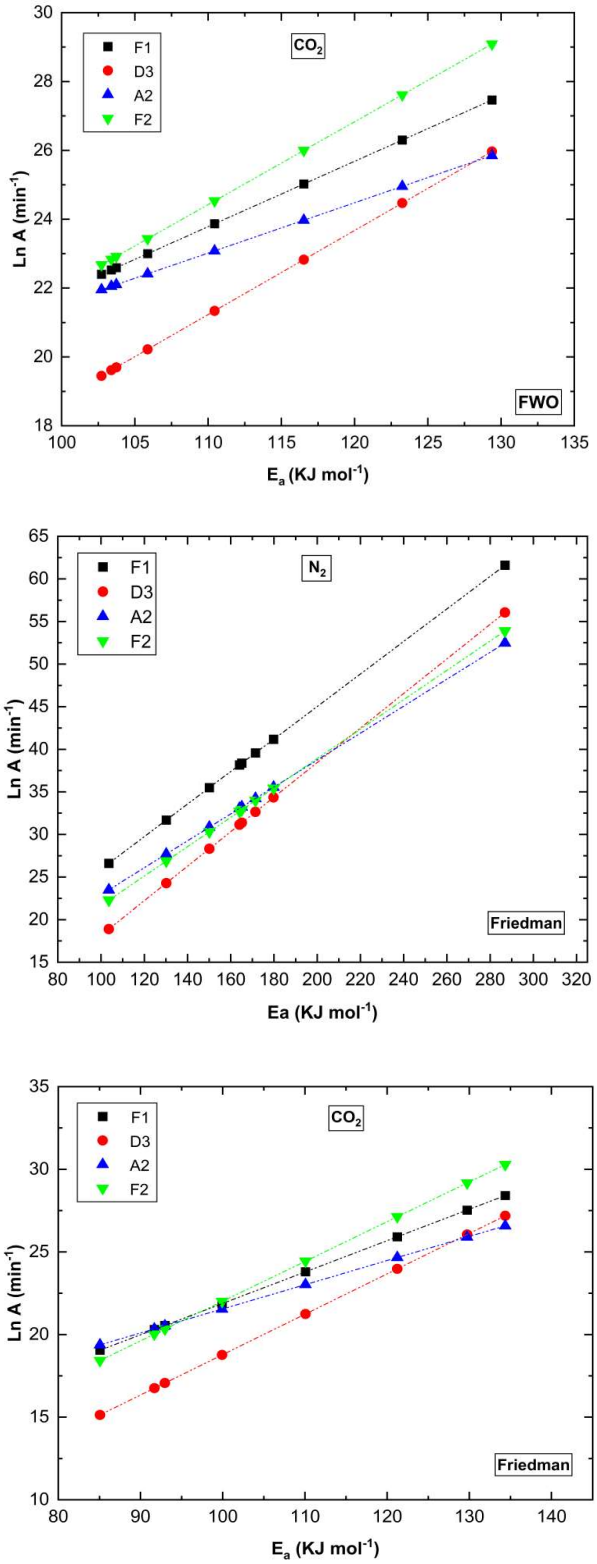

Fig. 3.12 Correlation between activation energy and pre-exponential factor under N_2 and CO_2 atmosphere using model-free methods

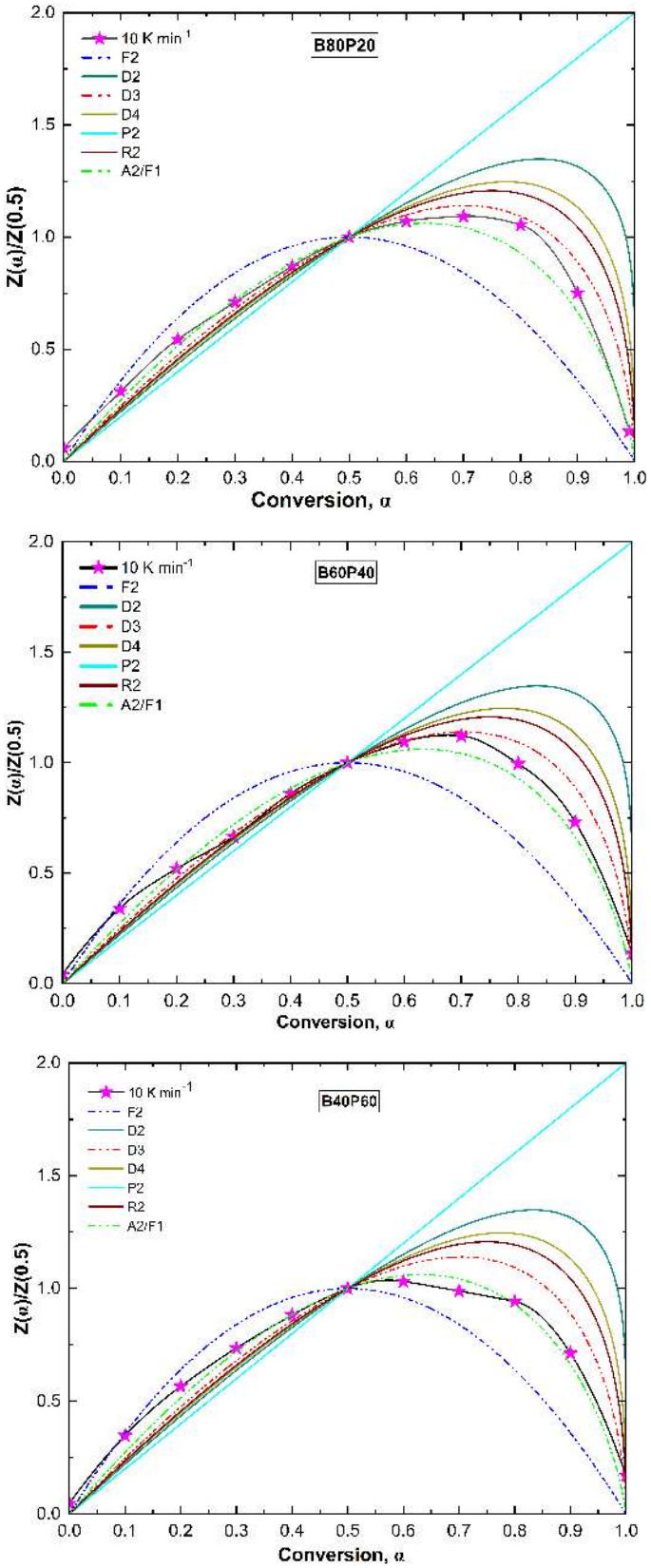

Fig. 3.13 $\frac{Z(\alpha)}{Z(0.5)}$ versus conversion for B80P20, B60P40, and B40P60 under CO_2 atmosphere

The experimental curve aligns with the second-order reaction model (F2) within a conversion range of 0 to 0.1 for the B80P20 fuel blend. Beyond this point, the curve transitions toward the nucleation model (A2) and the first-order reaction model (F1), continuing to follow these models until a conversion of 0.6. After this, the curve shifts toward the three-dimensional diffusion model (D3) between conversions of 0.6 and 0.8, although it does not completely overlap with this model. The curve then reverts to the A2/F1 trend, maintaining this profile until it reaches a conversion of 1.0. For the B60P40 formulation, the experimental data initially follows the F2 model from 0 to 0.1. From 0.1 to 0.2, the curve gradually transitions toward the A2/F1 models and continues this trajectory until it reaches the D3 model at a conversion of 0.3. The D3 model adheres to 0.3 to 0.7. After 0.7, the experimental curve starts to realign with the A2/F1 models, following this path until the conversion reaches 1.0. In the case of the B40P60 formulation, the experimental curve begins by following the F2 model from a conversion of 0 to 0.1. It then transitions toward the A2/F1 models, maintaining this alignment to a conversion of 0.6. Beyond 0.6, the curve tends to shift back toward the F2 model but ultimately returns to and follows the A2/F1 trend until it reaches a conversion of 1.0.

This analysis highlights the transitions between various reaction mechanisms at different conversion stages, offering a comprehensive understanding of the reaction pathways under CO_2 atmospheres for the blended fuel samples. By utilizing the most suitable reaction models identified for each blended fuel sample, the pre-exponential factor (A) values are determined based on the parameters of the compensation effect presented in Table 3.7. The calculated pre-exponential factor values for the different conversions of B80P20, B60P40, and B40P60 ranged from 23.39 to 30.64 min^{-1}, 33.53 to 40.85 min^{-1}, and 31.58 to 39.94 min^{-1}, respectively. The variations in pre-exponential factors across different stages of conversion exhibit the complex and heterogeneous nature of the blended fuel samples, suggesting the presence of a multi-step reaction mechanism during the thermal conversion process. In Fig

3.14, a clear linear relationship is observed between the activation energy and the pre-exponential factor. This linear correlation highlights the dependency of the pre-exponential factor on the activation energy in the context of the Arrhenius equation. The plot exhibits a strong linear trend, evidenced by a high coefficient of determination (R^2= 1), which confirms the reliability of the methods used to determine the kinetic parameters. This perfect fit not only validates the accuracy of the calculated kinetic values but also supports the applicability of the Arrhenius model to describe the reaction kinetics under the conditions studied [137].

Table 3.7 Comparison of activation energy of different blended samples

Compensation parameters	B80P20		B60P40		B40P60	
	a*	b*	a*	b*	a*	b*
F1	9.364	0.165	23.600	0.114	18.371	0.133
F2	13.667	0.142	21.445	0.123	16.613	0.140
D3	16.104	0.131	24.459	0.161	19.076	0.129
A2	15.407	0.134	23.601	0.114	18.368	0.133

The differences observed in the pre-exponential factor values indicate varying levels of reactivity within the system. Lower pre-exponential factor values suggest reduced reactivity, while higher values indicate enhanced reactivity. This reflects the dynamic nature of the thermal decomposition processes. These findings align with the insights provided by Yuan *et al.* (2017), which emphasize the relationship between the pre-exponential factor's magnitude and the reactivity of the process [145]. This variability highlights the complex reaction mechanisms involved in the thermal conversion of the blended fuel samples, emphasizing the processes intricacies.

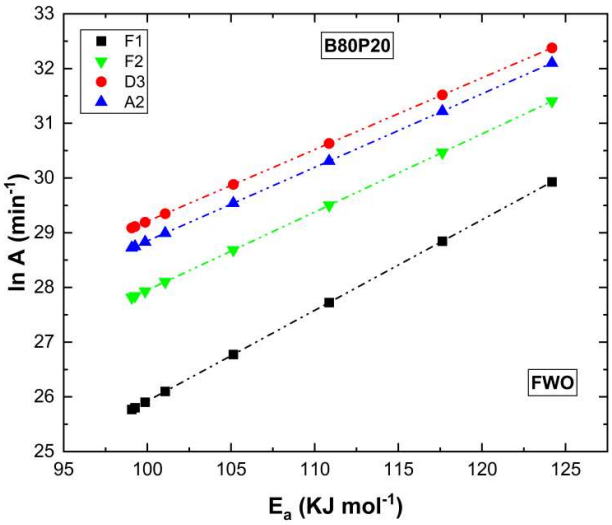
F1
F2
D3
A2
B80P20
FWO
ln A (min-1)
Ea (KJ mol-1)

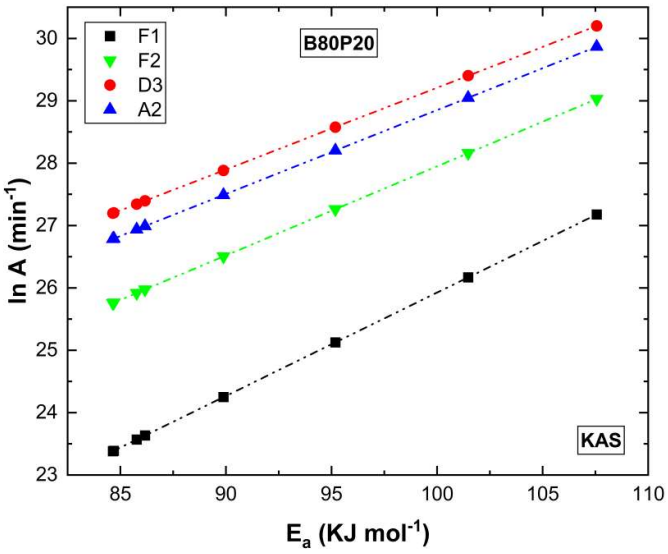
F1
F2
D3
A2
B80P20
KAS
ln A (min-1)
Ea (KJ mol-1)

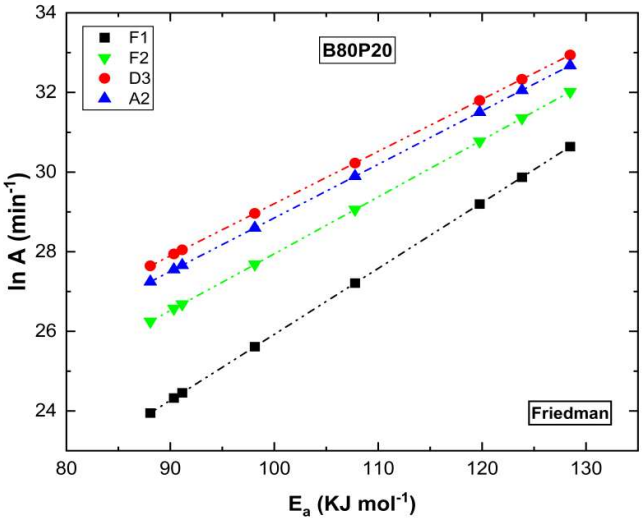
F1
F2
D3
A2
B80P20
Friedman
ln A (min-1)
Ea (KJ mol-1)

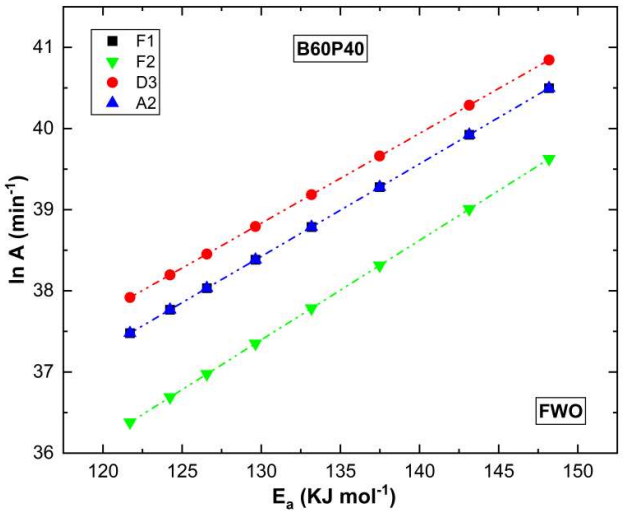
F1
F2
D3
A2
B60P40
FWO
ln A (min-1)
Ea (KJ mol-1)

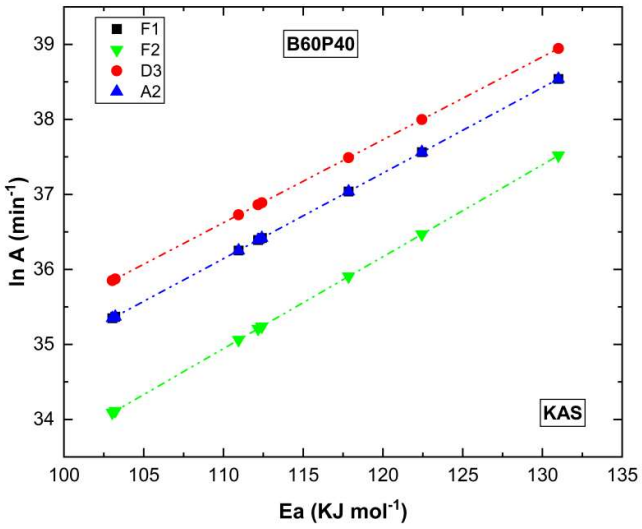
F1
F2
D3
A2
B60P40
KAS
ln A (min-1)
Ea (KJ mol-1)

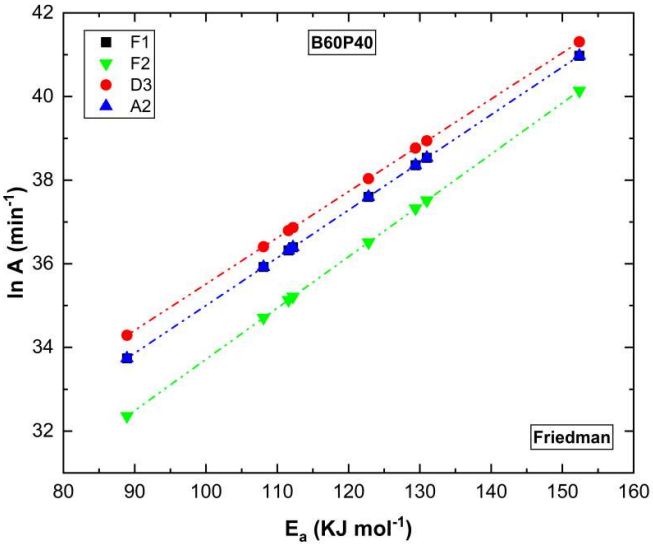
F1
F2
D3
A2
B60P40
Friedman
ln A (min-1)
Ea (KJ mol-1)

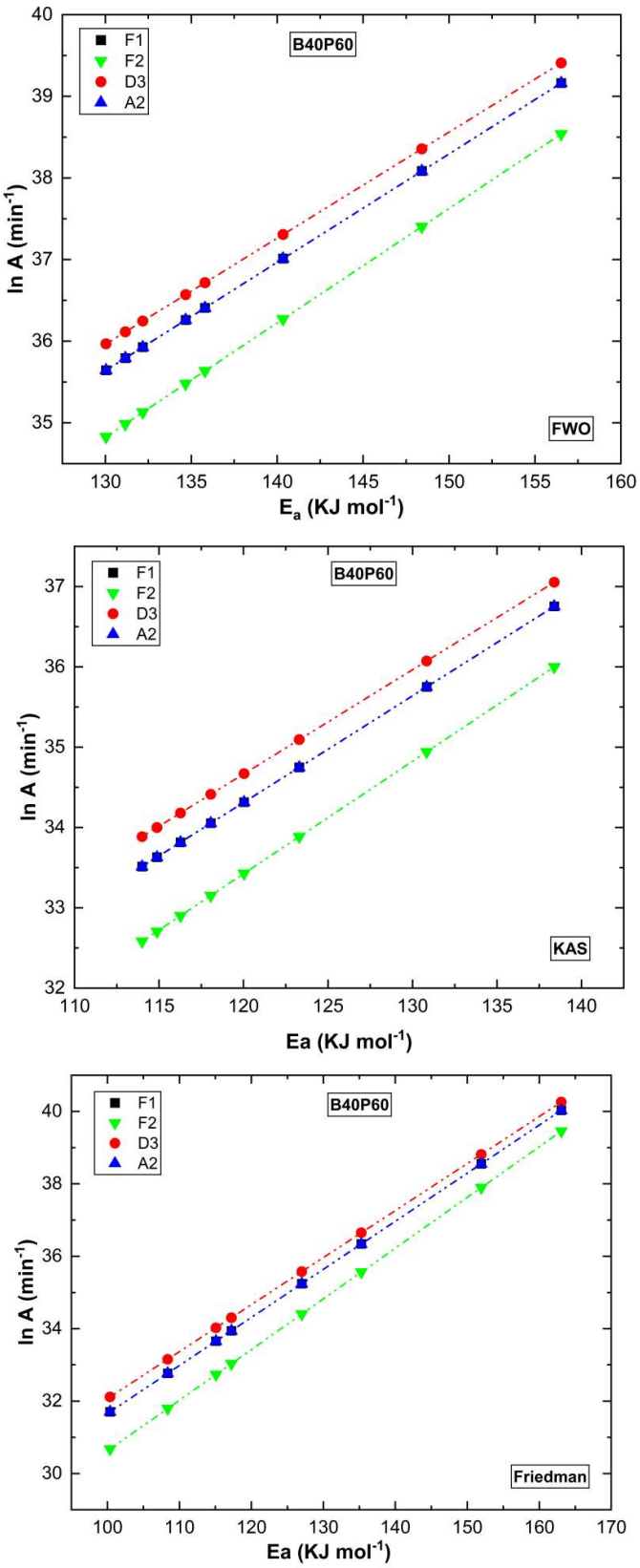

Fig. 3.14 Correlation between activation energy and pre-exponential factor of B80P0, B60P40, and B40P60 using model-free methods

3.1.4 Effect of N_2 and CO_2 on B. *tulda* char properties

Analysis of the char obtained from pyrolysis includes energy balance, physicochemical properties, and structural and elemental characterizations.

3.1.4.1 Mass and energy yield

The energy retained in the pyrolysis products can be estimated by analyzing the mass yield and higher heating value (HHV) on a dry and ash-free basis. Fig. 3.15 presents the distribution of mass and energy yields. It is found that the mass yield of B. *tulda* char decreased when pyrolyzed under carbon dioxide atmosphere compared to nitrogen atmosphere at the same temperature. The recorded mass yields are 46.26 % for pyrolysis in nitrogen (BCN) and 34.19 % for pyrolysis in carbon dioxide (BCC). The pyrolysis process for B. *tulda* also increased the higher heating value for both BCN and BCC. The energy yield for B. *tulda* char is determined to be 73.67 % for BCN and 59.08 % for BCC. Energy yield for biochar under N_2 atmosphere is greater despite having lower calorific value compared to CO_2 is due to higher yield of biochar under N_2 atmosphere. Similar findings have been reported by Maia *et al.* (2021) and Selvarajoo *et al.* (2020) [115, 146]. Furthermore, mass yield and energy yield are closely linked.

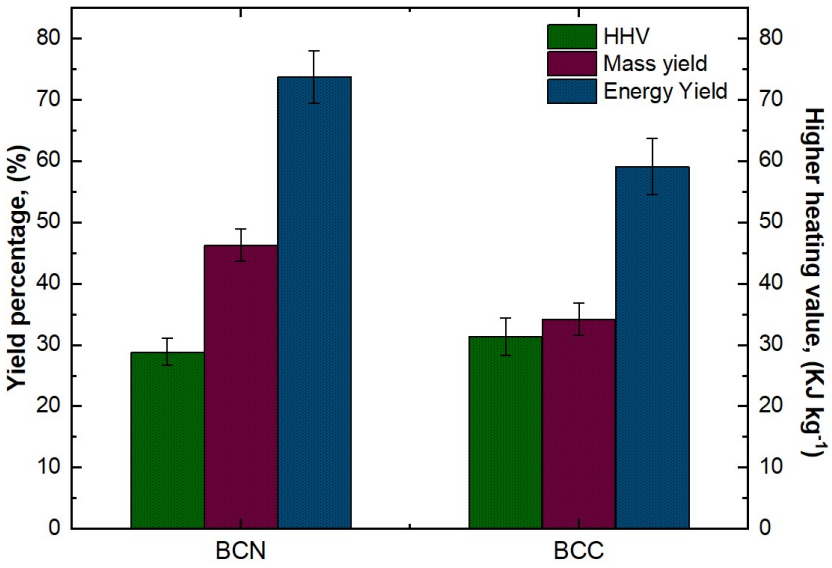

Fig. 3.15 HHV, mass yield and energy yield of BCN and BCC

Table 3.8 presents the physical and chemical characteristics of B. *tulda* and its associated chars, BCN and BCC. The analysis reveals that B. *tulda* contains a significant amount of volatile matter, measuring 72.4%, which makes it well-suited for thermochemical conversion processes. It has a low ash content of 2.41 % and a relatively high fixed carbon content of 16.85 %. Additionally, B. *tulda* has moisture content below 10%, specifically at 8.32%, which meets the biomass standards reported by Ounas *et al.* (2011) [39]. The low ash content and high fixed carbon percentage enhance B. *tulda* applicability in biofuels, while its relatively low moisture content supports efficient conversion. B. *tulda* also effectively minimizes expected NOx emissions due to the presence of low nitrogen content, a significant pollutant in syngas output. Proximate and ultimate analyses are conducted on the char derived from B. *tulda* (BCN and BCC) to study the impact of the pyrolysis atmosphere on their physical and chemical properties, as shown in Table 3.8. The pyrolysis process significantly alters the physical structure of the produced biochar. The effects of different pyrolysis atmospheres on volatile matter and calorific value are evident at the studied temperatures. The volatile content decreased notably, with BCN measuring 11.74% and BCC at 8.95%, indicating a substantial reduction due to the aromatization process and the thermal degradation of lignocellulosic components.

The ultimate analysis of BCN and BCC demonstrated how the pyrolysis atmosphere influences the elemental composition of the char. Both types of char showed an increase in carbon content, accompanied by a decrease in hydrogen and oxygen levels. This trend signifies an enhancement of carbonization reactions. Notably, BCC had higher carbon content than BCN, indicating that the specific reaction atmosphere improved the carbonization process by facilitating de-oxygenation and dehydrogenation reactions, resulting in the production of carbon-reach char. The elemental composition of the B. *tulda* char is consistent with the findings of Yi *et al.* (2022) [120]. The increased carbon content in the B. *tulda* char led to higher calorific values, reaching 25.36 $MJkg^{-1}$ for BCN and 29.44 $MJkg^{-1}$ for BCC.

According to Lee *et al.* (2017), the H/C and O/C ratios can be used to quantitatively assess the degree of carbonization and polarity in carbon products [57]. Additionally, different atmospheres as part of the pyrolysis medium during the pyrolysis process can influence these parameters. The molar ratio of H/C for B. *tulda* char generated under N_2 and CO_2 atmosphere is 0.23 and 0.26 respectively. This suggests that highly condensed structures, such as aromatic rings, are present in both carbon products. The B. *tulda* char produced in N_2 atmospheres has a higher O/C molar ratio of 0.16 compared to 0.11 for the biochar generated in CO_2 atmosphere. This indicates that the biochar produced in the N_2 atmosphere may be more polar or hydrophilic than the biochar produced in the CO_2 atmosphere [58].

Table 3.8 Physicochemical properties of B. *tulda,* BCN and BCC

Fuel samples	B. *tulda*	BCN	BCC
Proximate analysis (wt %) (db)			
Moisture content (MC)	8.32±1.21	1.72±0.4	1.37±1.03
Volatile matter (VM)	72.42±3.8	11.74±1.1	8.95±0.87
Ash content (AC)	2.41±0.8	4.28±0.9	4.97±1.14
Fixed carbon (FC)*	16.85	82.26	84.71
Ultimate analysis (wt %) (db)			
Carbon (C)	45.47±3.7	81.23±4.11	85.16±3.29
Hydrogen (H)	6.08±1.6	1.56±0.75	1.79±0.89
Nitrogen (N)	2.0±0.8	0.41±0.08	0.53±1.0
Oxygen (O)*	46.45	16.80	12.52
Atomic ratio H/C	1.60	0.23	0.26
Atomic ratio O/C	0.76	0.16	0.11
Higher Heating Value (MJ/kg)	17.85±1.4	25.36±2.2	29.44±3.05
Compositional analysis (%)			
Cellulose	50.16±1.13		
Hemi-cellulose	25.43±0.92	-	-
Lignin	21.08±0.55	-	-
Extractives*	3.33	-	-
*db: dry basis, * estimate by the difference*			

3.1.4.2 FTIR analysis

Fig. 3.16 presents the FTIR peaks of BCN and BCC. Table 3.9 presents the FTIR wave number range of B. *tulda*, BCN and BCC respectively. The intensity of the absorption of alcoholic or phenolic-OH groups, observed at 3450 cm^{-1} in B. *tulda*, decreases in both BCN and BCC due to the breakdown of oxygen-containing functional groups during the hydration reaction. However, the absorption peak for -OH in BCC is stronger than in BCN. The peak around 2920 cm^{-1} represents the asymmetric stretching vibration of CH_2 for aliphatic groups, while the peak near 2850 cm^{-1} corresponds to a symmetric stretching peak in alkenes. The intensity of both peaks reduces with the addition of CO_2, which is attributed to the catalytic effect during the cracking of aliphatic C-H functional groups [147]. The characteristic peak at 1745 cm^{-1}, which corresponds to C=O stretching, is more prominent in BCC than in BCN. Additionally, the absorption peak at 1630 cm^{-1} indicates aromatic C=C ring stretching vibration, which decreases with pyrolysis due to interactions with basic functional groups. Furthermore, BCC shows a high proportion of aromatic constituents and a relatively low presence of aliphatic constituents, indicating enhanced aromatic properties and reduced aliphatic characteristics. As a result, bamboo char pyrolyzed under CO_2 atmosphere demonstrates greater resistance to degradation compared to bamboo char produced under N_2 atmosphere [40].

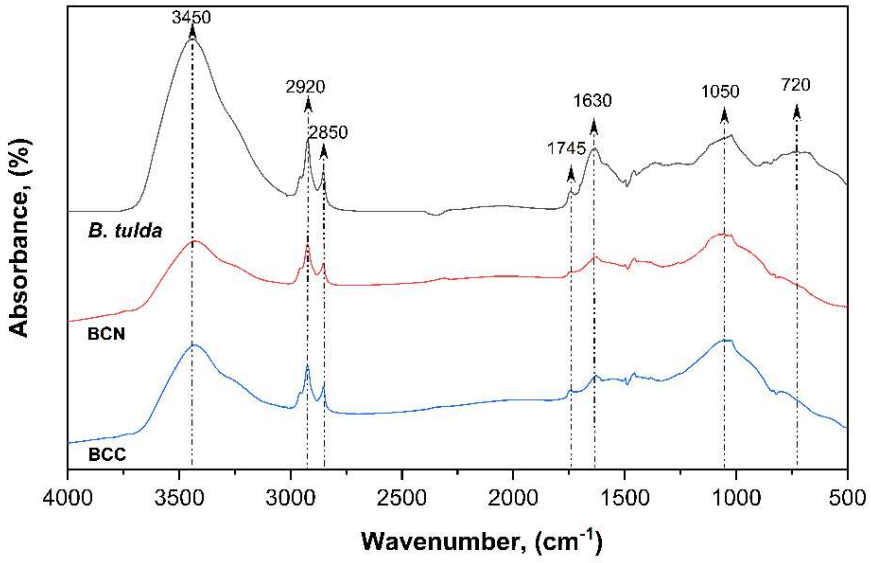

Fig. 3.16 FTIR of *B. tulda*, BCN and BCC

Table 3.9 FTIR range of B. *tulda*, BCN and BCC

Wave number cm^{-1}	Range	Functional group	Appearance
3450	3550-3200	O-H stretching	strong, broad
2920	3000-2840	C-H stretching	medium
2850	2860-2800	O-H stretching	weak
1745	1750-1735	C=O stretching	weak
1630	1662-1626	C=C stretching	medium
1050	1250-1020	C=O stretching	medium
720	730-665	C=C bending	narrow, broad

3.1.4.3 XRD analysis

X-ray Diffraction (XRD) analysis is performed to identify the presence of various crystalline materials that influence the characteristics of B. *tulda* char for its applications. The analysis involved plotting the intensity of the diffracted beam against the Bragg angle (2θ), within the range of 10° to 80°. The XRD results for BCN and BCC are shown in Fig. 3.17, with the 2θ values compared to those found in the JCPDS database and other published literature. In the XRD pattern, peaks at 2θ values of 20.87° and 26.36° indicated the presence of SiO_2 in both BCN and BCC. However, the intensity of SiO_2 is lower in BCC compared to BCN. Additionally, peaks at 28.57°, 40.56°, and 50.01° in BCN, along with a peak at 28.62° in BCC, suggest the crystalline phase of KCl. In the case of BCN, multiple peaks indicate a higher concentration of potassium (K) and chlorine (Cl), consistent with values reported by Sahoo *et al.* (2021) [148]. Furthermore, $CaCO_3$ is observed at a 2θ value of approximately 30.55° in BCN, but this peak disappeared in BCC, likely due to complete decomposition or conversion to CaO at the peak of 67.48°. CO_2 assisted in the complete decomposition of crystalline structure. This observation is supported by the findings of Basumatary *et al.* (2021) [149]. The XRD patterns of BCN and BCC demonstrate that the pyrolysis atmosphere can create variations in the intensity of the peaks of the different components.

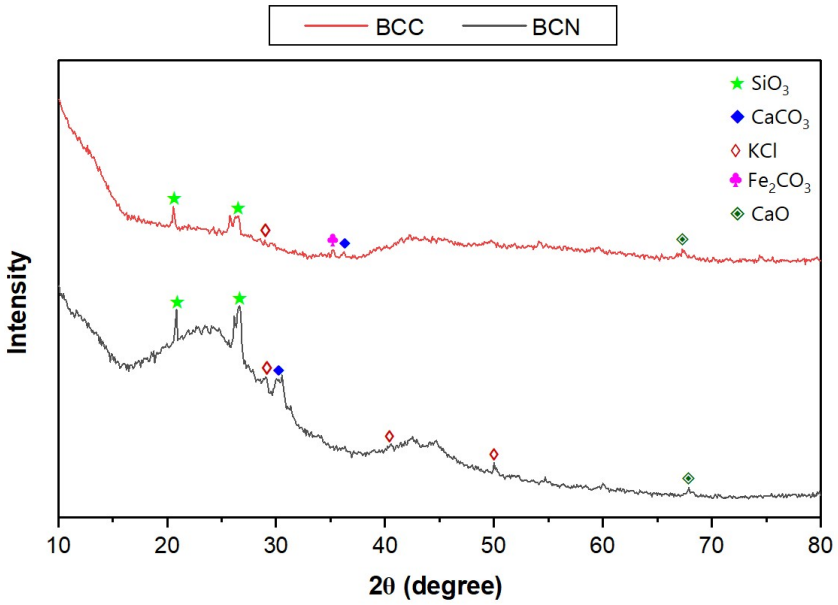

Fig. 3.17 XRD analysis of BCN and BCC

3.1.4.4 SEM-EDX analysis

The results presented in Fig. 3.18 highlight distinct structural differences between BCN and BCC produced under N_2 and CO_2 pyrolysis atmospheres. The morphology of BCN exhibits a porous and well-organized structure, while BCC exhibits a collapsed pore structure that resembles channels. This channel-like formation in BCC is attributed to the development of an aromatic structure. During pyrolysis under CO_2 atmosphere, the intense release of volatile substances and the thermal breakdown of B. *tulda* further contributed to this channel-like morphology. These observations are consistent with findings reported by Sahoo *et al.* (2021) [148]. During the pyrolysis process under N_2 atmosphere, biomass undergoes devolatilization, which creates porosity. The resulting pores vary in size and are classified as micropores (5-30 µm), mesopores (30-75 µm), and macropores (>75 µm) [150, 151]. The pore size distributions are analyzed to investigate how the pyrolysis atmosphere influences the characteristics of biochar. The results indicated that biochar produced in a N_2 atmosphere had pore sizes ranging from 5 to 11.32 µm. In contrast, biochar generated in a CO_2 atmosphere exhibited larger pores, ranging from 12.73 to 36.37 µm.

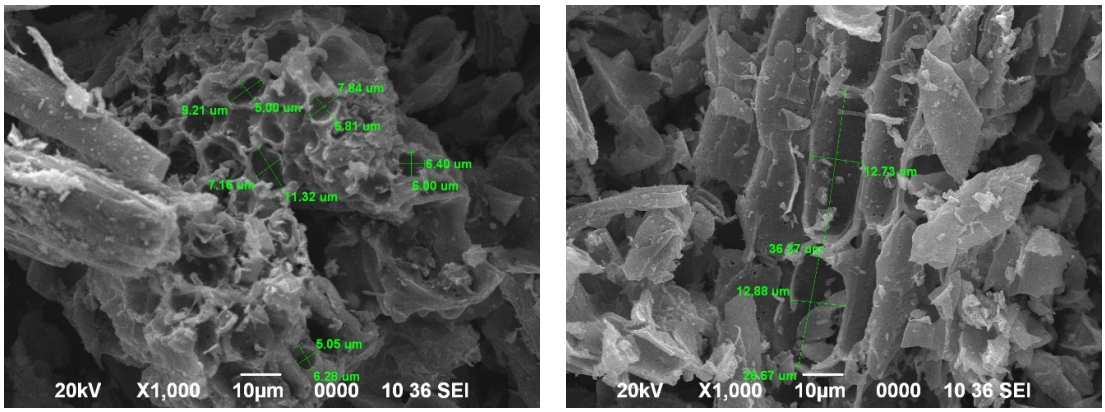

Fig. 3.18 SEM analysis BCN and BCC

This indicates that the N_2 atmosphere produces biochar with better-developed pore structures, while the CO_2 atmosphere yields a higher number of pores. Furthermore, the porosity of the biochar increases when the pyrolysis atmosphere is switched to CO_2. Additionally, CO_2 acts as a weak oxidizing agent, promoting the formation and release of additional volatile compounds that contribute to developing pores on the char surface. The process follows a hierarchical order, where in the first step CO_2 interacts with the volatile fractions released during thermal degradation. Once the volatile matter is depleted, the CO_2 selectively alters the morphology of the biochar [152]. The heterogeneous reaction between the sample surface and the surrounding environment of CO_2 explain the formation of larger pores compared to those found in the N_2 atmosphere [58]. Several researchers have also linked changes in biochar morphology with the gasification effects of CO_2 that may occur during pyrolysis [57, 40].

The elemental composition of biochar derived from B. *tulda* (referred to as BCN and BCC) is analyzed under N_2 and CO_2 atmospheres using Energy Dispersive X-ray Spectroscopy (EDX), as illustrated in Fig. 3.19. The pyrolysis process revealed the presence of various compounds on the surface of the char, including potassium (K), magnesium (Mg), calcium (Ca), silicon (Si), phosphorus (P), and aluminum (Al) [153]. Notably, the char produced under a CO_2 atmosphere contains a higher percentage of potassium than that produced under N_2

atmosphere. While potassium can contribute to fouling and slagging, blending B. *tulda* biochar with coal or petcoke may enhance the combustion or gasification process by promoting thermal cracking. Furthermore, the calcium, potassium, and phosphorus in biochar can enrich the soil with essential nutrients [154].

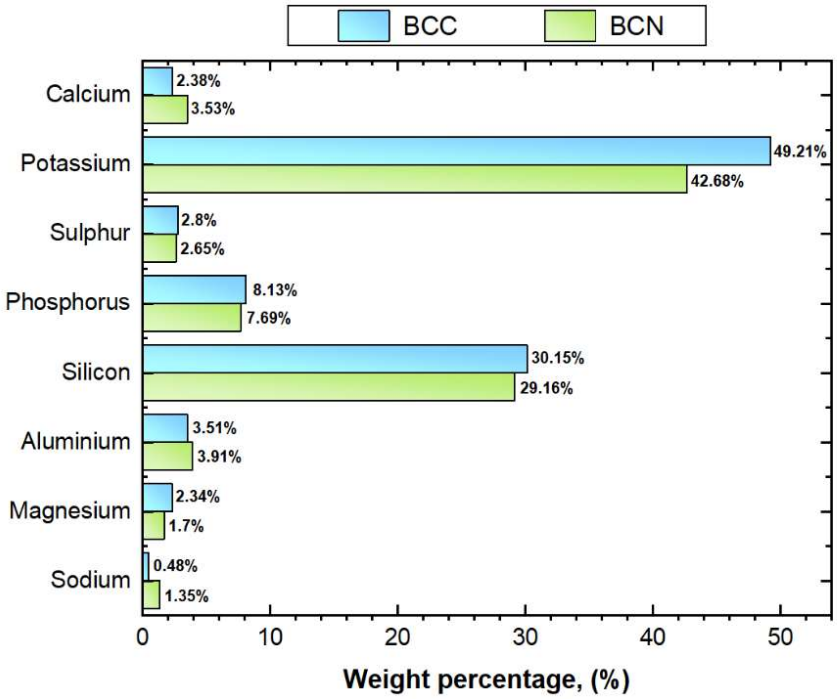

Fig. 3.19 EDX analysis of BCN and BCC

3.2 Summary

This study aimed to investigate the thermal degradation of B. *tulda* using a Thermogravimetric Analysis (TGA) analyzer to determine the kinetic parameters under N_2 and CO_2 atmosphere. The addition of CO_2 reduced the activation energy of bamboo compared to its baseline value under N_2 atmosphere. Additionally, pyrolysis of B. *tulda* is carried out in a fixed-bed pyrolysis system to produce biochar in N_2 and CO_2 atmospheres. The results indicated that the activation energies are 160.05 kJmol^{-1} under N_2 atmosphere and 105.51 kJ mol^{-1} under CO_2 atmosphere. Furthermore, blending of B. *tulda* with petcoke reduced the activation energy and improved thermal conversion efficiency. The activation energies for the B80P20, B60P40, and B40P60 blends are 101.66 kJ mol^{-1}, 122.23 kJ mol^{-1}, and 129.30 kJ

mol^{-1}, respectively, all of which are lower than that of pure petcoke. The catalytic effect of alkali and alkaline earth metals in B. *tulda* facilitates better thermal degradation. The thermal degradation process of B. *tulda* is complex and can be described by multiple models, with A2, D3, F1, and F2 being the most suitable. The lnA values under N_2 atmosphere vary between 22.82 and 56.01 min^{-1}, while the values under CO_2 atmosphere range from 17.99 to 27.16 min^{-1}. Additionally, the experimental conversion curves for the B80P20, B60P40, and B40P60 blends exhibited distinct transitions among various reaction models (F2, A2, F1, and D3). This reveals the different reaction mechanisms occurring at various stages of thermal degradation in CO_2 atmospheres. By utilizing the most appropriate reaction models, the pre-exponential factor (A) values are determined ranging from 23.39 to 30.64 min^{-1} for B80P20, from 33.53 to 40.85 min^{-1} for B60P40, and from 31.58 to 39.94 min^{-1} for B40P60.

The variations observed in the thermal conversion process highlight its complexity and dynamic nature. Higher the activation energy indicates increased reactivity. Upon analyzing the physical and chemical properties of the B. *tulda* char, it is found that the char produced under N_2 atmosphere had higher energy content (73.67 %) than that produced under CO_2 atmosphere (59.08 %). During pyrolysis, both bamboo char (BCN and BCC), showed increased carbon content and decreased hydrogen and oxygen content, indicating enhanced carbonization. The atomic ratio also revealed higher aromaticity and thermal stability.

Bamboo char is particularly rich in potassium, magnesium, calcium, and sodium, which can enhance its reactivity in co-gasification or co-firing scenarios with other fuels like coal or petcoke. Additionally, BCC demonstrated high levels of aromatic compounds and a relatively lower presence of aliphatic compounds. This indicates pronounced aromatic qualities and reduced aliphatic characteristics, leading to bamboo char pyrolyzed under CO_2 atmosphere having greater degradation resistance than that produced under N_2 atmosphere. The synergistic effect of these properties can be advantageous in gasification or combustion

processes. Moreover, regardless of the pyrolysis atmosphere, bamboo char maintains high carbon content and calorific value, rendering it a promising feedstock for gasification and an alternative to fossil fuels. These findings suggest that bamboo char from B. *tulda* could be a renewable resource for biofuels and a potential substitute for fossil fuels.